

อนุภาคระดับนาโนเมตรของทองคำบับเงินเตรียมด้วยปฏิกิริยาแทนที่เกลแวนิก

นาย ประเสริฐ ศรีประสิทธิ์

วิทยานิพนธ์นี้เป็นส่วนหนึ่งของการศึกษาตามหลักสูตรปริญญาวิทยาศาสตรมหาบัณฑิต

สาขาวิชาเคมี ภาควิชาเคมี

คณะวิทยาศาสตร์ จุฬาลงกรณ์มหาวิทยาลัย

ปีการศึกษา 2554

ลิขสิทธิ์ของจุฬาลงกรณ์มหาวิทยาลัย

GOLD NANOPARTICLES ON SILVER SURFACE PREPARED BY GALVANIC
REPLACEMENT REACTION

Mr. Prasert Sornprasit

A Thesis Submitted in Partial Fulfillment of the Requirements
for the Degree of Master of Science Program in Chemistry

Department of Chemistry

Faculty of Science

Chulalongkorn University

Academic Year 2011

Copyright of Chulalongkorn University

Thesis Title GOLD NANOPARTICLES ON SILVER SURFACE
PREPARED BY GALVANIC REPLACEMENT
REACTION
By Mr. Prasert Sornprasit
Field of Study Chemistry
Thesis Advisor Associate Professor Sanong Ekgasit, Ph.D.
Thesis Co-advisor Associate Professor Chuchaat Thammacharoen

Accepted by the Faculty of Science, Chulalongkorn University in Partial
Fulfillment of the Requirements for Master's Degree

.....Dean of the Faculty of
Science
(Professor Supot Hannongbua, Dr.rer.nat.)

THESIS COMMITTEE

.....Chairman
(Assistant Professor Warinthorn Chavasiri, Ph.D.)

.....Thesis Advisor
(Associate Professor Sanong Ekgasit, Ph.D.)

.....Thesis Co-advisor
(Associate Professor Chuchaat Thammacharoen)

.....Examiner
(Associate Professor Vithaya Ruangpornvisuti, Dr.rer.nat.)

.....External Examiner
(Associate Professor Vittaya Amornkitbamrung, Ph.D.)

ประเสริฐ ศรีประสิทธิ์ : อนุภาคระดับนาโนเมตรของทองคำบนผิวเงินเตรียมโดยปฏิกิริยาแทนที่แกลวานิก. (GOLD NANOPARTICLES ON SILVER SURFACE PREPARED BY GALVANIC REPLACEMENT REACTION) อ. ที่ปริกษาวิทยานิพนธ์หลัก: รศ. ดร. สมอง เอกสิทธิ์, อ. ที่ปริกษาวิทยานิพนธ์ร่วม: รศ. ชูชาติ ธรรมเจริญ), 59 หน้า.

เทคนิคใหม่สำหรับการสร้างโครงสร้างที่มีความซับซ้อนในระดับไมโครและนาโนเมตรของทองคำประกอบด้วยฟิล์มที่มีโครงสร้างคล้ายปะการัง คล้ายเข็ม คล้ายสวนหิน และ โครงสร้างคล้ายปะการังที่มีรูพรุนระดับไมโครและนาโนเมตรโดยใช้ปฏิกิริยาแทนที่แกลวานิกระหว่างโลหะเงินและไอออนของทองคำได้ถูกรายงาน โครงสร้างที่มีความซับซ้อนระดับไมโครและนาโนเมตรของทองคำสามารถควบคุมด้วยการปรับเปลี่ยนความเข้มข้นของไอออนของทองคำ ระยะเวลาการจุ่ม ความเข้มข้นของไอออนของคลอไรด์ ความเป็นกรด-ด่าง รังสีอัลตราโซนิก วิวัฒนาการของโครงสร้างที่มีความซับซ้อนในระดับไมโครและนาโนเมตรของทองคำถูกสังเกตด้วยกล้องจุลทรรศน์แบบส่องกราด (SEM) ควบคู่กับเทคนิคการวิเคราะห์รังสีแบบ EDS เทคนิคเอกซเรย์ดิฟแฟรกชัน (XRD) และกล้องจุลทรรศน์ การสร้างชั้นเอพิแทกซ์ของฟิล์มทองบนพื้นผิวเงินถูกรบกวนด้วยตะกอนระดับไมโครและนาโนเมตรของซิลเวอร์คลอไรด์ การโตร่วมกันของซิลเวอร์คลอไรด์และฟิล์มทองที่สร้างจากปฏิกิริยาแกลวานิกเหนี่ยวนำให้เกิดฟิล์มผสมระดับไมโครและนาโนเมตรของทองคำและซิลเวอร์คลอไรด์บนพื้นผิวของเงิน ซิลเวอร์คลอไรด์และไอออนซิลเวอร์คลอไรด์คอมเพล็กซ์ (AgCl_2^-) แสดงบทบาทสำคัญในการเกิดวิวัฒนาการของโครงสร้างระดับไมโครและนาโนเมตรของทองคำที่คล้ายปะการังและคล้ายเข็ม รังสีอัลตราโซนิกสามารถเหนี่ยวนำให้เกิดการแยกออกแบบอัตโนมัติที่ส่วนต่อประสานของฟิล์มของทองคำและซิลเวอร์คลอไรด์ที่สร้างจากปฏิกิริยาแกลวานิก โครงสร้างที่มีความซับซ้อนในระดับไมโครและนาโนเมตรของทองคำปรากฏทันทีที่ซิลเวอร์คลอไรด์ที่โตร่วมกันถูกกำจัด โครงสร้างคล้ายปะการังที่มีรูพรุนระดับไมโครและนาโนเมตรของทองคำสามารถเพิ่มสัญญาณรามานของโรดามีน 6 จี (R6G) และคริสตัลไวโอเลต (CV) ความเข้มข้น 10^{-6} โมล

ภาควิชา.....เคมี.....ลายมือชื่อนิสิต.....
 สาขาวิชา.....เคมี.....ลายมือชื่อ อ. ที่ปริกษาวิทยานิพนธ์หลัก.....
 ปีการศึกษา.....2554.....ลายมือชื่อ อ.ที่ปริกษาร่วม.....

5272683023 : MAJOR CHEMISTRY

KEYWORDS : COMPLEX GOLD MICRO/NANOSTRUCTURES/ GALVANIC
REPLACEMENT REACTION/ SERS

PRASERT SORNPRASIT: GOLD NANOPARTICLES ON SILVER
SURFACE PREPARED BY GALVANIC REPLACEMENT REACTION.
ADVISOR: ASSOC. PROF. SANONG EKGASIT, Ph.D., CO-ADVISOR:
ASSOC. PROF. CHUCHAAT THAMMACHAROEN, 59 pp.

A novel technique for fabricating complex gold micro/nanostructures including coral-liked, needle-liked, Zen stone-liked gold micro/nanostructures, and coral-liked gold micro/nanoporous film using galvanic replacement reaction between a sacrificed silver metal and gold (III) ion have been reported. The complex gold micro/nanostructures could be controlled by adjustable gold ion concentration, immersion time, chloride ion concentration, pH, and ultrasonic radiation. The structural evolutions of gold micro/nanostructures were observed by scanning electron microscope (SEM) with energy dispersive X-ray spectroscopy (EDS), X-ray diffraction (XRD), and digital camera. The epitaxial growth of gold film on the silver surface was disturbed by the precipitated AgCl micro/nanoparticles. The co-development of AgCl precipitates and galvanic generated Au film induced a formation of Au/AgCl micro/nanocomposites on silver surface. AgCl and AgCl_2^- played important roles on the evolution of coral-liked, needled-liked gold nanostructures. The ultrasonic also induced an auto-detachment of the galvanic generated film along the Ag/AgCl interface. The complex gold nanostructures with nanoporous morphology were realized once the co-developed AgCl was removed. The coral-liked gold micro/nanoporous express high SERS detection up to 10^{-6} M rhodamine 6G (R6G) and crystal violet (CV).

Department :chemistry..... Student's Signature

Field of Study :chemistry..... Advisor's Signature

Academic Year :2011..... Co-advisor's Signature

ACKNOWLEDGEMENTS

I would like to express my sincere gratitude to Associate Professor Dr. Sanong Ekgasit and Associate Professor Chuchaat Thammacharoen for wholeheartedly provide the useful guidance, understanding, training and teaching the theoretical background and technical skills during my research.

I would like to thank Assistant Professor Dr. Warinthorn Chavasiri, Associate Professor Dr. Ruangpornvisuti, and Associate Professor Dr. Vittaya Amornkitbamrung for usefully substantial suggestions as the thesis committee.

Warmest thanks to my colleagues and organization: Sensor Research Unit, Department of Chemistry, Faculty of Science, Chulalongkorn University, and all good friends for the suggestions and spiritual supports throughout this research.

I would also especially like to thank partial financial supports in my research: The Office of the National Research Council of Thailand (NRCT), Center of Innovative Nanotechnology Chulalongkorn University (CIN-CU), National Center of Excellence for Petroleum, Petrochemicals and Advanced Materials (CE PPAM).

Whatever shortcomings in the thesis remain, they are the sole responsibility of the author

Above all, I am profoundly grateful to my parents and endearing family for all their loves, understanding, support, and encouragement during the whole period of my study.

CONTENTS

	Page
ABSTRACT IN THAI.....	iv
ABSTRACT IN ENGLISH.....	v
ACKNOWLEDGEMENTS.....	vi
CONTENTS.....	vii
LIST OF TABLES.....	x
LIST OF FIGURES.....	xvi
LIST OF ABBREVIATIONS.....	xvii
CHAPTER I INTRODUCTION.....	1
1.1 Anisotropic structures for functional materials.....	1
1.2 The objective of this research.....	2
1.3 Scopes of research.....	2
1.4 The benefits of this research.....	2
CHAPTER II THEORETICAL BACKGROUND.....	3
2.1 Gold nanostructures synthesis.....	3
2.1.1 Physical method.....	3
2.1.1.1 Arc discharge method.....	3
2.1.1.2 Aerosol method.....	3
2.1.1.3 Laser ablation/irradiation in liquid method.....	4
2.1.2 Chemical method.....	4
2.1.2.1 Seed-mediated method.....	5
2.1.2.2 Polyol synthesis method.....	6
2.1.2.3 Photochemical synthesis method.....	7
2.1.2.4 Sonochemical method.....	9
2.1.2.5 Galvanic replacement reaction method.....	10

	Page
2.2 Characterization techniques.....	13
2.2.1 Scanning electron microscope.....	13
2.2.2 Energy-dispersive X-ray spectrometer.....	13
2.2.3 Raman spectroscopy.....	14
2.2.4 UV-visible spectroscopy.....	14
 CHAPTER III EXPERIMENTAL SECTION.....	 15
3.1 Chemicals and materials.....	15
3.2 Synthesis of coral-liked gold nanostructures.....	15
3.3 Synthesis of needle-liked gold nanostructures.....	16
3.4 Ultrasonic assisted fabrication of coral-liked gold nanoporous.....	16
3.5 Dissolution of silver chloride by ammonia treatment.....	17
3.6 Characterizations.....	17
3.6.1 Scanning electron microscope (SEM).....	17
3.6.2 X-ray powder diffraction (XRD).....	17
3.6.3 Surface enhances Raman scattering (SERS) measurement.....	17
3.6.4 UV-visible spectroscopy.....	18
 CHAPTER IV RESULTS AND DISCUSSION.....	 19
4.1 Synthesis of coral-liked gold nanostructures.....	19
4.1.1 The concentration effect of Au ³⁺ solution on gold structures..	24
4.1.2 Time dependent evolution of CLGNs.....	28
4.1.3 AgCl under layer formation on the Au/AgCl composites.....	30
4.1.4 The pH of Au ³⁺ solution influence on gold structures.....	32
4.2 Synthesis of NLGNs.....	35
4.2.1 The effect of NaCl on NLGNs.....	35
4.2.2 Micro-channel on AgCl layer.....	36
4.2.3 Time dependent evolution of NLGNs.....	38

	Page
4.2.4 X-ray diffraction (XRD) pattern of the CLGNs and NLGNs...	40
4.3 Synthesis of standing coral-like gold nanoporous.....	41
4.3.1 Optical property of Au/AgCl composites.....	41
4.3.2 UV-visible change of Au ³⁺ solution on galvanic replacement reaction.....	42
4.3.3 The morphology of CLGPs.....	43
4.3.4 Elemental composition of Au/AgCl composites and CLGPs..	44
4.3.5 Proposed circle galvanic replacement reaction mechanism....	46
4.3.6 Surface enhances Raman scattering activity of CLGPs.....	48
CHAPTER V CONCLUSIONS.....	51
REFERENCES.....	52
VITAE.....	59

LIST OF TABLES

Table		Page
2.1	summarize galvanic replacement reaction method for metal film creation.....	12
4.1	Assignment of Raman bands of the SERS spectrum of R6G.....	49
4.2	Assignment of Raman bands of the SERS spectrum of CV.....	50

LIST OF FIGURES

Figure	Page
2.1	Schematic diagram of the arc discharge system (A) instrument component (B) mechanism of plasma generated gold nanoparticles.... 4
2.2	Schematic diagram of the laser ablation method..... 4
2.3	(a) TEM images of gold nanorods prepare by growth solution with various aspect ratios..... 5
2.4	(A) Low- and (B) high-magnification SEM micrographs of slightly truncated silver nanocubes synthesized with the polyol process. (C) TEM images of a purified sample of silver nanowires..... 7
2.5	A schematic illustrating the reaction pathways that leads to noble-metal nanoparticles having different shapes..... 8
2.6	Schematic illustration of the reduction process of metal salts in the presence of a polymer or coordination compound..... 8
2.7	Schematic diagrams summarizing all steps of structural evolutions involved the galvanic replacement reaction of a silver nanocube and an aqueous AuCl_4^- solution. (A) The galvanic replacement reaction start to dissolve at the site that with high surface energies as oxidation reaction. The electron from the reaction was migrated to surface then reduce AuCl_4^- to Au atom. Incomplete layer of gold film epitaxial deposited on the face of a cube (B) continues galvanic replacement reaction between Ag and AuCl_4^- formed a partially hollow nanostructure. (C) Formation of nanoboxes with a uniform and homogeneous wall. In the step A, B, and C the alloying occur underlying silver surface (D) initiation of dealloying and morphological reconstruction of the Au-Ag nanobox; (E, F) continuation of dealloying, together with the formation of pores in the wall; and (G) fragmentation of the porous Au nanobox. The cross-sectional views correspond to the plane along dashed lines..... 11

Figure	Page
2.8 Schematic drawing SEM of the column showing electron gun, lenses the electron deflection, and electron detector.....	13
4.1 UV-visible spectra of 5,000 ppm Au ³⁺ diluted to 10 ppm non reaction and 30 min galvanic replacement reaction.....	20
4.2 (A, B) Low magnification SEM micrographs of silver globules observed before and after galvanic replacement reaction 30 min, (inset) digital image of silver globules.....	20
4.3 (A, B) Energy dispersive X-ray spectra of Au/AgCl layer with 30 min. before and after ammonia treatment, (inset) SEM micrographs of corresponding condition.....	21
4.4 Elemental distributions at 30 min galvanic replacement reaction of silver globules and 5,000 ppm of Au ³⁺ . (A1) SEM micrographs of galvanized silver globule surface before ammonia treatment, (A2-A4) Au, Ag, and Cl maps before ammonia treatment of silver surface. (B1-B4) corresponding SEM micrograph and EDS maps after remove AgCl by ammonia treatment.....	22
4.5 Schematic diagram of galvanic replacement reaction shows Au/AgCl co-depositions on sacrificed silver surface, <i>i.e.</i> , as the film become thicker. Equation (5, 6) oxidation and reduction reaction occurred as anode and cathode site. Equation (7) shows total galvanic replacement reaction. Common ion effects of AgCl are also depicted in equation (8).....	23
4.6 AgCl dissolution process by ammonia treatment (NH ₃).....	23
4.7 (A) Digital images of Au ³⁺ concentration at 0, 50, 100, 500, 1,000, and 5,000 ppm. (B) Corresponding condition (A) of silver globule after 30 min of galvanic replacement reaction.....	24

Figure	Page
4.8 Structural developments of CLGNs due to concentration of Au ³⁺ with 30 min reaction time. (A1-A6 and B1-B6) SEM micrographs of Au/AgCl composites and Au nanostructures increase the concentrations, 0, 50, 100, 500, 1,000, and 5,000 ppm Au ³⁺ at 30 min of reaction time.....	26
4.9 Elemental analysis of galvanized layer on silver surface with 0, 50, 100, 500, 1,000, and 5,000 ppm Au ³⁺ solution at 30 min. (A) ratio of Ag/Cl (B, C) Au and Ag before and after ammonia treatment.....	28
4.10 (A1-A6) Time dependent evolution of Au/AgCl co-deposited on silver globules surface by galvanic replacement reaction, silver globules and 5,000 ppm Au ³⁺ at 1, 5, 10, 20, 30, and 60 min respectively, (B2-B6) structural development of gold after removing silver chloride by ammonia treatment. (C) Cross section vertical panorama SEM micrograph on CLGNs with 30 min reaction time.....	31
4.11 (A, C, and E) SEM micrographs of cross section galvanized silver surface with 5,000 ppm Au ³⁺ at 5, 30, and 60 sec reaction time before ammonia treatment.....	32
4.12 Structural developments of coral-liked, Zen stone-liked gold nanostructures, and gold thin film due to pH of Au ³⁺ solution with 30 min reaction time. (A, B, and C) SEM micrographs of galvanized silver surface of 5,000 ppm of Au ³⁺ solution with pH 0, 7, and 14, reaction time 30 min respectively. (1and 2) SEM micrographs were compared after ammonia treatment.....	33
4.13 Atomic ratios of Ag/Au and Cl/Au on galvanized-layer at pH 0, 7, and 14 (A, B) before and after ammonia treatment.....	34
4.14 EDS mapping of elemental Zen stone liked-gold microstructures (A) SEM micrograph, (B, C, and D) Cl, Ag, and Au mapping.....	34

Figure	Page
4.15 (A, B) SEM micrographs of NLGNs before and ammonia treatment (C, D) SEM micrographs with back scattering detector (E) corresponding SEM micrograph with (D).....	35
4.16 (A1-A6) Structural developments of NLGNs by galvanic replacement reaction, silver globules and 5,000 ppm of Au ³⁺ solution was mixed 0, 0.1, 0.3, 0.5, 1, 2 M NaCl at 30 min respectively. (A2-A6) structure developments of NLGNs after remove AgCl by ammonia treatment.....	37
4.17 (A, B, and C) SEM micrographs of galvanized silver was removed AgCl with 0, 0.5, and 10 % w/v NH ₃ . (1 and 2) SEM magnification take with 5,000x and 10,000x.....	38
4.18 (A1-A6) Time dependent of NLGNs by galvanic replacement reaction between silver globules and 5,000 ppm Au ³⁺ was mixed 2 M NaCl at 0, 5, 10, 20, 30 and 60 min respectively. (A2-A6) corresponding of NLGNs after removing AgCl by ammonia treatment.....	39
4.19 XRD patterns of CLGNs and NLGNs after ammonia treatment.....	40
4.20 Digital images of snap shot video of galvanic reaction (A) 5,000 ppm Au ³⁺ before galvanic replacement reaction (B-E) galvanic replacement reaction at 00:00.000, 00:0.083, 00:09.167, 00:20.242, and 07:13.917 reaction time (sec).....	42
4.21 (A, B) UV-visible spectra of 5,000 ppm Au ³⁺ diluted to 10 ppm before and after galvanic replacement reaction. Image inset: Digital image of Au ³⁺ solution.....	43
4.22 CLGPs synthesis by using ultrasonic assisted, (A, C, and E) SEM micrographs CLGPs before ammonia treatment and (B, D, and F) after galvanic replacement reaction.....	44
4.23 Pore size distribution of CLGPs show combinations of micro and nanoporous on structures, (inset) SEM micrograph captured with high resolution.....	45

Figure	Page
4.24 EDS spectra of Au/AgCl composites and CLGPs.....	46
4.25 Schematic diagram of circle galvanic replacement reaction show the film is automatically detached from the sacrificed silver plate, <i>i.e.</i> , as the film becomes thicker. The mechanism of the nanoporous gold film development included: (A) supply/regeneration of a clean Ag surface (B) rapid epitaxial growth of Au film on the clean Ag surface (C) precipitation and formation of AgCl precipitates on Au film (D) formation of interpenetrated Au/AgCl nanocomposite (E) development of AgCl underlay (F) ultrasonic assisted detachment of the (galvanic generated) interpenetrated Au/AgCl nanocomposite film with AgCl underlay from the silver plate. The detachment occurs at the interface between Ag plate and the AgCl underlay. The ultrasonic assisted auto-detachment enables a self-initiated formation of clean Ag surface of the silver plate.....	47
4.26 SERS of 1×10^{-5} and 1×10^{-6} Molar of R6G on CLNPs compared with 1×10^{-3} Molar of R6G on glass slide.....	48
4.27 SERS of 1×10^{-5} and 1×10^{-6} Molar of CV on CLNPs compared with 1×10^{-3} Molar of R6G on glass slide.....	49

LIST OF ABBREVIATIONS

CLGNs	: Coral-liked gold nanostructures
NLGNs	: Needle-liked gold nanostructures
CLGPs	: Coral-liked gold nanoporous
SERS	: Surface enhanced Raman scattering
nm	: Nanometer
AgCl	: Silver chloride
AgCl_2^-	: Silver chloride ion complex
Ag	: Argentum (silver)
AuCl_4^- , Au^{3+}	: Gold(III) chloride
NaBr	: Sodium bromide
NaCl	: Sodium chloride
HCl	: Hydrochloric acid
Au	: Gold
R6G	: Rhodamine 6G
CV	: Crystal violet
CTAB	: Alkyltrimethylammonium bromides
CTAC	: Cetyltrimethylammonium chloride
CPC	: Cetylpyridinium chloride
PVP	: Poly (vinyl pyrrolidone)
μL	: Microlite (volume)
ppm	: Parts per million (concentration, mg/L)
M	: Molar (concentration, mol/L)
SEM	: Scanning electron microscopy
UV-vis	: UV-visible
LMCT	: Ligand-to-metal-charge-transfer
UV	: Ultraviolet (light)
EDS	: Energy-dispersive X-ray spectrometer

CHAPTER I

INTRODUCTION

1.1 Anisotropic structures for functional materials.

Recently, metal nanostructures are of interest for researchers due to their differentially unique properties with bulk materials and promising applications in catalyst e.g., oxidative coupling, electrocatalytic [1, 2], biosensor e.g., solid support for immobilizing biomolecules in modern biosensor technology [3-5], optical sensing [6], surface enhanced Raman scattering (SERS) e.g., single molecule and single particle detection [7, 8]. Those applications will be needed appropriately properties of nanostructures that dependent on their sizes, shapes, compositions, and patterns. Nowadays, the anisotropic structures such as nanorod and nanowire [9], nanoplate [10, 11], octahedral [12, 13], nanostar, nanoflower, dendritic, branched [14-17], nanocage, and nanoframes [18, 19] was developed using any methods. The anisotropic structures have been created by seed-mediated method, polyol method, galvanic replacement reaction method, photochemical method, electrochemical method, template-mediated method and so on [20].

However, anisotropic nanomaterials cannot use fruitful applications, particularly SERS. Size and shape of the metal nanomaterials influence to SERS performance, enhancements process of SERS based on the field enhancement at sharp edges, corners, and interstitials of nanoparticles [21-23]. Assembly of anisotropic nanostructures as film could be increased an enhancement of SERS and changed optical property of nanomaterials [24, 25]. Furthermore, the galvanic replacement reaction was one of the methods that created complex structures as film.

In this work, methods for synthesizing complex gold structures including coral-liked gold nanostructures (CLGNs), needle-liked gold nanostructures (NLGNs) and standing coral-liked gold micro/nanoporous (CLGPs) by using galvanic replacement reaction were developed. The complex gold structures occurred after cleaning process. The gold structures derived from galvanic replacement reaction that could be controlled by various parameters *i.e.*, concentration of gold (III) ion, reaction time, additive ion. Furthermore, in this method we synthesized complex gold

structures and controlled by AgCl precipitates and AgCl_2 as template as well as mobile template at ambient condition. Finally, the standing CLGPs were demonstrated an approach to detect low concentration of rhodamine 6G (R6G) dye and crystal violet (CV) using a small volume (1 μL).

1.2 The objectives of this research

1.2.1 To develop the new method for synthesizing complex gold micro/nanostructures on silver surface via galvanic replacement reaction.

1.2.2 To study structural formation of complex gold structures due to the effect of Au^{3+} concentration, pH of Au^{3+} solution, reaction time and ultrasonic radiation.

1.3 Scopes of research

1.3.1 Developing a novel method for synthesizing complex gold structures.

1.3.2 Investigating the effects of gold (III) ion concentration, reaction time, chloride ion, and ultrasonic radiation on the structural evolution

1.3.3 Proposing the growth mechanism of complex gold structures.

1.3.4 Examining the SERS property of complex gold structures.

1.4 The benefits of this research

1.4.1 Novel method for synthesizing complex gold micro/nanostructures without capping agent and stabilizer is established.

1.4.2 Complex gold micro/nanostructures for SERS applications are manifested.

CHAPTER II

THEORETICAL BACKGROUND

2.1 Gold nanostructures synthesis

There are many methods for synthesizing metal nanostructures. Mostly, the fabrication methods of metal nanostructures can be divided into two main types, bottom-up and top-down approaches. Top-down approach was started from standard bulk materials and reduced to nanometer size with physical mechanization of those materials. Mostly bulk materials were evaporated at high temperature and dented to nanomaterials. But the bottom-up approaches started from atom or molecule and built up to nanometer size of materials using chemical reaction and physical interaction. Generally, methods of synthesis metal nanostructures have two important aspects, chemical and physical methods.

2.1.1 Physical method

2.1.1.1 Arc discharge method (ADM)

The large amount of energy estimated temperature of 1500-5000 K at gap distance between the electrodes was generated by stable pulse voltage about 135 volts [26-28]. The particle size of gold nanoparticles in the range of 2-40 nm with spherical shape on surface of electrode was melted and vaporized. Schematic diagram of the arc discharge system generated gold nanoparticles by plasma between gaps of electrode shown in Fig 2.1. The advantage of ADM method could be generated gold nanostructures without chemical surfactants and stabilizers at water or ethanol solution. Spherical structures were generated in this method. However, this method was applied to synthesize single-walled carbon nanotubes [28].

2.1.1.2 Aerosol method

Aerosol method produced gold nanoparticle by heating high purity gold placed inside a tube furnace at 1650 °C under carrier nitrogen gas. As the gold vapor at heated zone was condensed into particles and coagulated resulting in a wide size distribution. Charger device as UV light creating free electrons then charge

the neutral particles to positive and negative particles. Finally, wide size distribution gold nanoparticle was classified by their aerodynamic diameter at differential mobility analyzer by balancing the force from an electric field [29].

2.1.1.3 Laser ablation/irradiation in liquid method

Laser ablation with gold plates in the liquid medium with stabilizer can be produced various gold nanostructures (nanoparticles, nanocubes, nanorods, nanocomposites, etc.). The fabrication and modification of nanomaterials in liquid based on laser irradiation has become a rapidly growing field .Fig 2.2 shows schematic diagram of the laser ablation method. The particles size can be controlled by changing the laser intensity and wavelength [30].

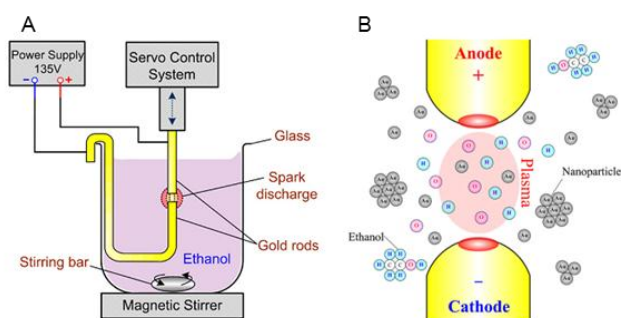


Figure 2.1 Schematic diagram of the arc discharge system (A) instrument component (B) mechanism of plasma generated gold nanoparticles [26].

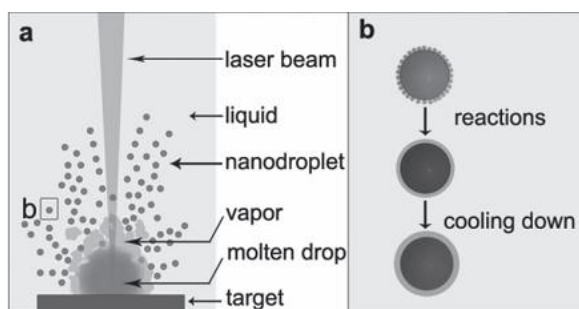


Figure 2.2 Schematic diagram of the laser ablation method [30].

2.1.2 Chemical method

The chemical method is mostly popular among chemists in the few years. The standard protocol for synthesis gold nanostructures using chemical method

can be divided into chemical reaction and electrochemical reaction follows by type of reaction. The chemical reaction synthesized nanoparticles in liquid phase using metal salt and reducing agent. Borohydride reduction was classical method for synthesis of gold nanoparticles that the reactions occur rapidly causing the immediate nucleation of metal particles [31]. Recently, anisotropic noble nanomaterials (e.g., gold, silver, platinum, and palladium) are of interest in the few years due to those structures. More complicated synthetic method of anisotropic nanomaterials has been remarkable than isotropic nanomaterials. Seed-mediated method, polyol method, photochemical method, electrochemical method, galvanic replacement reaction method was generated anisotropic nanomaterials.

2.1.2.1 Seed-mediated method

The seed-mediated growth process is a widely use anisotropic nanostructures. This method including two steps, 1st step: seed fabrication process by conventional reduction reaction was created. Sodium borohydride is a simple reducing agent for generation nanoparticle. 2nd step: seed grew into the anisotropic structures then metal morphology using grows solution. Surfactant and mild reducing agent are mainly active species in the growth solution for controlling the growing of metal structures. Fig 2.3 shows gold nanorods preparing by growth solution with various aspect ratios. On the other hand, anisotropic structures could be dictated by varying parameter e.g., amount of concentration of seed, additive agent.

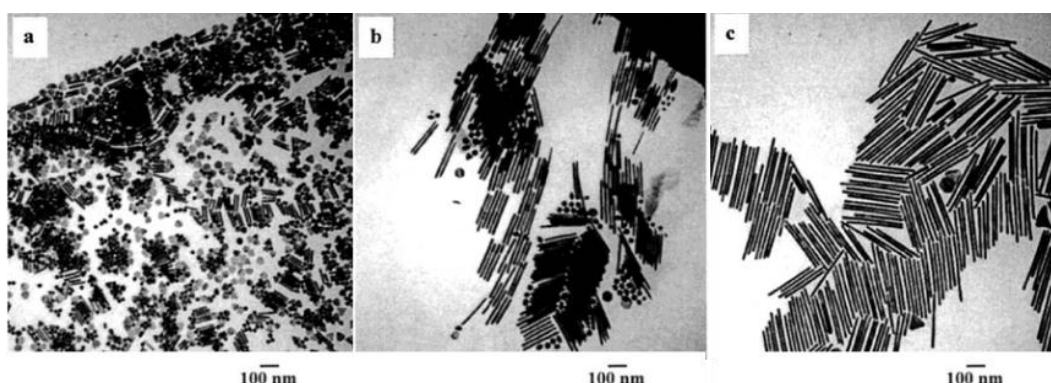


Figure 2.3 (a) TEM images of gold nanorods prepare by growth solution with various aspect ratios [32].

Preparation of gold nanorods with aspect ratios of 4.6 ± 1.2 , 13 ± 2 , and 18 ± 2.5 nm by seeding growth approach is controlled by varying the ratio of seed to metal salt [32]. The gold nanorods were demonstrated with three steps of seed-mediated growth method using different surfactants, alkyltrimethylammonium bromides (CTAB) and cetylpyridinium chloride (CPC). The longer chain lengths of the surfactant tail are producing longer gold nanorods. "Zipping" mechanism was proposed which surfactant bilayer stabilized on the gold surface by Van der Waals. In general, the length of the surfactant chain increased which induced the increasing of aspect ratio of gold nanoparticles [33]. The seed-mediated deposition of Au nanorods directly on glass surfaces using CTAB was reported. The concentration of The AuCl_4^- is the key factor of the experiment that average length and aspect ratio of the nanorods increases with increasing AuCl_4^- concentration [34]. However, seed-mediated synthesis method could be changed the gold structures from cubic to trisoctahedral, and rhombic dodecahedral structures using cetyltrimethylammonium chloride (CTAC), surfactant, NaBr, and aromatic additives [35, 36]. Seed-mediated co-reduction shows new idea for synthesis gold palladium shape-controlled alloy nanostructures [37].

2.1.2.2 Polyol synthesis method

Polyol reduction is one of the methods to synthesize anisotropic structures with controllable shapes and optical properties as shown in Fig. 2.4. In a typical synthesis, ethylene glycol acts as reductant generating metal atoms from a salt precursor at an elevated temperature ($100-160$ °C) [38-40]. The formation of nanostructures with controlled shapes is facilitated by adding capping agent e.g., poly (vinyl pyrrolidone) (PVP). Uniform shape of the quasi-spherical gold particles prepared using polyol reduction between AuCl_4^- in a PVP-ethylene glycol solution. The solution was heated up to the desirous reaction temperature (100°C to the boiling point of ethylene glycol). The 0.1 to 0.4 μm showed the ranges size of the powder [40]. Large quantities of silver nanocubes with edge length of 175 nm and nanowires with diameters of $30-40$ nm, and lengths up to 50 μm was synthesized by ethylene glycol in the presence of PVP as capping reagent. The silver cubes use as sacrificial

templates for single-crystalline nanoboxes and hollow polyhedra of gold synthesis by galvanic replacement reaction [38, 39]. Different seeds (single-crystal, cuboctahedrons, and cubes seeds) can be grown to nanostructures with different shapes by controlling growth rates as shown in Fig. 2.5. For example, a single-crystal seed can grow into an octahedron or cube, single-crystal cuboctahedrons and cubes grow to nanorods with octagonal cross sections and nanobars with rectangular cross sections, multiply twinned seeds with a decahedral shape can be directed to grow into rods or nanowires with a pentagonal cross section, and plate-like seeds grow into hexagonal and then eventually triangular plates [41].

2.1.2.3 Photochemical synthesis method

Photochemical synthesis gold nanoparticles as well as general photochemistry are similar to the previous method with chemical reductant. Generally, the method using a soft templates, macromolecular polymers, dendrimers or surfactants to form micelles or reverse micelles, control size and structures of gold nanostructures. Under UV irradiation conditions, intramolecular photoreduction generated reducing agent and also were protective action of polymer or coordination compound for the reduction process of Au (III) ions as shown in Fig.2.6 [42].

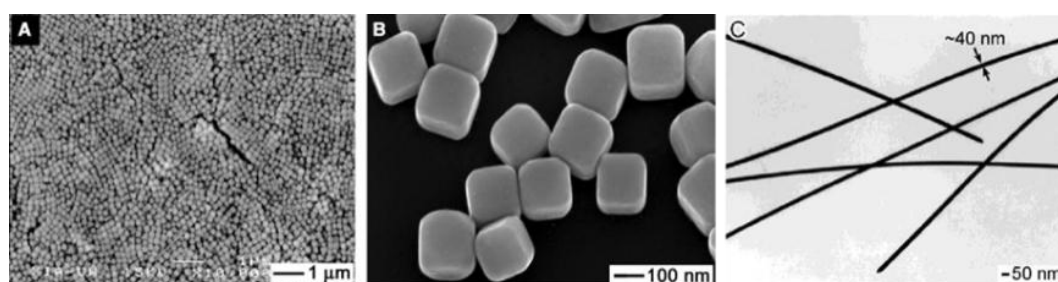


Figure 2.4 (A) Low- and (B) high-magnification SEM micrographs of slightly truncated silver nanocubes synthesized with the polyol process. (C) TEM images of a purified sample of silver nanowires [38, 39].

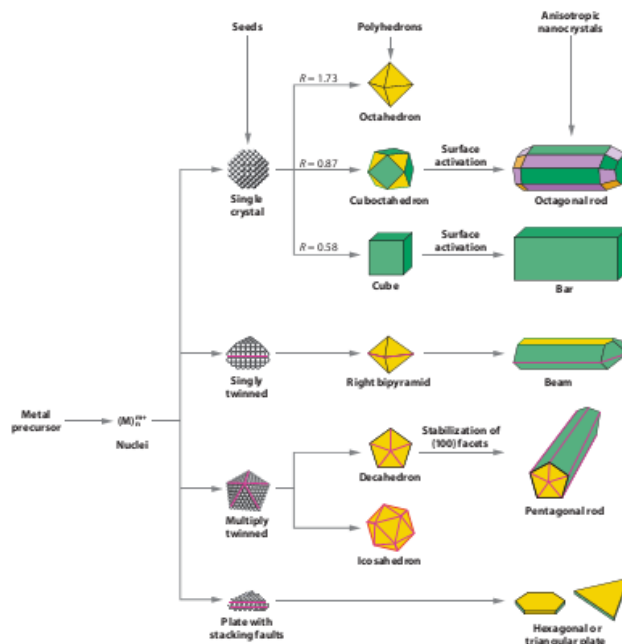


Figure 2.5 A schematic illustrating the reaction pathways that leads to noble-metal nanoparticles having different shapes. [41].

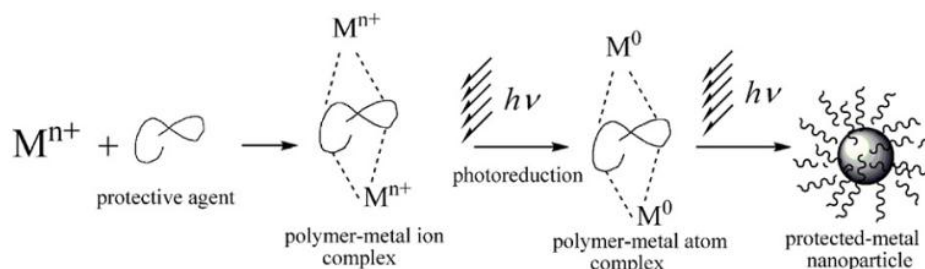


Figure 2.6 Schematic illustration of the reduction process of metal salts in the presence of a polymer or coordination compound [42].

Rod-liked gold colloidal was prepared by UV irradiation (253.7 nm light) in the presence of hexadecyltrimethylammonium chloride (HTAC) as a template. At the concentration of HTAC 30 wt % containing with 5-40 mmol dm⁻³ of AuCl₄⁻ will be formed to rods while prolong the irradiation time. The results of reaction shown the length of rod liked gold particles were increased depending on irradiation time [43]. Synthesis of polygonal gold nanoparticles, the method does not use either surfactants or polymers. Gold nanoparticles with particle size of 25-200 nm was reduced by odium oxalate under illumination of a mercury lamp [44].

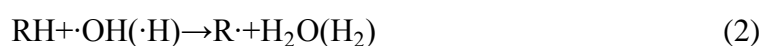
2.1.2.4 Sonochemical method

Chemical and physical effects of ultrasonic irradiation are known to prepare metal particles (Ag, Pd, Au, Pt and Rh) with nanometer size. There are three pathways of different reduction under sonication [45-47].

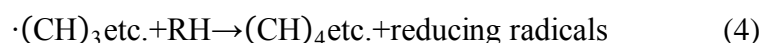
(i) Reduction by H atoms.



(ii) Reduction by secondary reducing radicals.



(iii) Reduction by radicals from pyrolysis of the additives.



* RH: stabilizer such as a surfactant or polymer

However, the surfactant and reducer free of gold nanoparticles were synthesized using a high-frequency (950 kHz) ultrasound (in the absence of any stabilizing, capping and reducing agents). Addition of NaCl, HCl and increasing AuCl_4^- concentration could be enhanced plates formation that caused by the specific adsorption on crystal facets e.g. (1 1 1) facets of Cl^- [48]. Ultrasound could be assisted fusion of gold nanoparticles (average diameter 25 ± 7 nm) to dumbbell-liked, worm-liked, and ring-liked gold nanostructures [49]. The ultrasonic method created of extremely high pressures (~ 108 Pa) and temperatures (~ 5000 K). Ultrasonic cavitation is known to provide very rapid heating/cooling rates (e.g., greater than 2109Ks^{-1} and may be as large as 1013Ks^{-1}) leading to dramatic changes of material crystalline structures [50]. However, the physical effect of ultrasound is the most effective mean for cleaning technologies e.g. ultrafiltration membranes [51]. The effect of a cleaning process parameters within an ultrasonic bath results of cleaning process controlled hydrodynamic cavitation in the shear layer using ultrasonic [52].

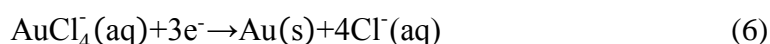
2.1.2.5 Galvanic replacement reaction method

The galvanic replacement reaction was simple method for creating complex structures by consuming the more sacrifice metal component. Spontaneous redox reaction occurred if standard reduction potential of total reaction was positive. In the case of Ag metal and AuCl_4^- , the standard reduction potential of $\text{AuCl}_4^-/\text{Au}$ pair (0.99 V vs standard hydrogen electrode, SHE) is higher than that of the Ag^+/Ag pair (0.80 V vs SHE), According to previous report when a silver metal was galvanized by gold (III) ion, the following reactions occurred [53, 54].

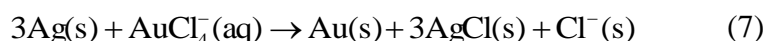
(i) Oxidation reaction.(anode site)



(ii) Reduction reaction (cathode site)



(iii) Redox reaction



Different Ag nanostructures were transformed metal nanostructures with hollow interiors with different morphologies including cubic nanoboxes, cubic nanocages, nanorings, nano-boxes, single-walled nanotubes, and multiple-walled nanoshells or nanotubes [53-55]. The galvanic replacement reaction mechanism generated nanobox and nanocages as shown in Figure 2.7. However, the galvanic replacement reaction could be generated complex gold nanostructures as film on metal substrate. Ge and Si mostly use as metal substrate under HF and Au (III) ions solution. HF play importance role induce oxidation reaction of galvanic replacement, Au (III) ions were reduced to gold atom growing to complex gold nanostructures on metal substrate as shown in Table 1.

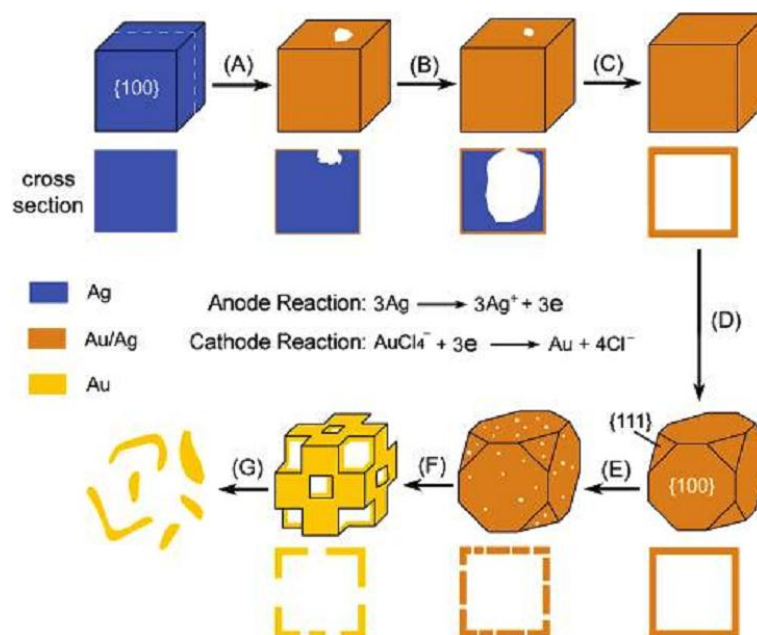
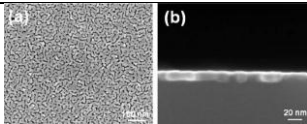
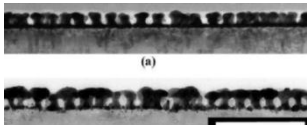
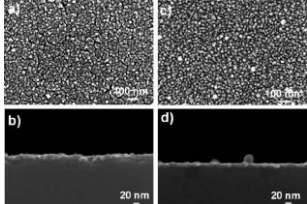
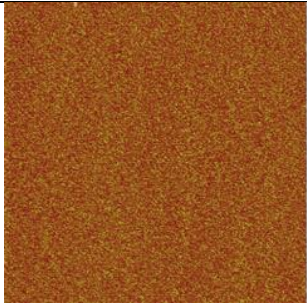
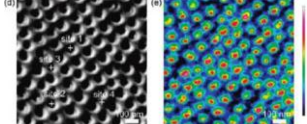


Figure 2.7 Schematic diagrams summarizing all steps of structural evolutions involved the galvanic replacement reaction of a silver nanocube and an aqueous AuCl_4^- solution. (A) The galvanic replacement reaction start to dissolve at the site that with high surface energies as oxidation reaction. The electron from the reaction was migrated to surface then reduce AuCl_4^- to Au atom. Incomplete layer of gold film epitaxial deposited on the face of a cube (B) continues galvanic replacement reaction between Ag and AuCl_4^- formed a partially hollow nanostructure. (C) Formation of nanoboxes with a uniform and homogeneous wall. In the step A, B, and C the alloying occur underlying silver surface (D) initiation of dealloying and morphological reconstruction of the Au-Ag nanobox; (E, F) continuation of dealloying, together with the formation of pores in the wall; and (G) fragmentation of the porous Au nanobox. The cross-sectional views correspond to the plane along dashed lines [53].

Table 2.1 Summarized galvanic replacement reaction method for metal film creation

Author /Year	Chemical	Structures	Figure
S.Y. Sayed et.al [56] (2009)	Si, KAuCl ₄ xH ₂ O, HF	Gold film on Si	
Y. Wang et.al [57] (2009)	Si, NaAuCl ₄ , HF,	mushroom- shaped gold nanopillars (50 nm)	
S. Y. Sayed et.al [58] (2010)	Ge (111), KAuCl ₄ xH ₂ O, HF	Gold films on germanium	
A. Gutes et.al [59] (2011)	Si, HF, and KAuCl ₄	Ultrasmooth Gold Thin Films	
X. Zhang et.al [60] (2011)	Si, HF, HAuCl ₄	Pseudo hexagonal arrays	

2.2 Characterization techniques

2.2.2 Scanning electron microscope

Scanning electron microscope (SEM) was widely used for observation and characterization of the material on a nanometer to micrometer scale. The signal was generated from interaction of electron beam and simple include secondary electron and backscattered electron. Those signals were processed and displayed to imaging signal that obtained from specific emission volumes of simple. The image signals of the secondary and backscattered electron of great interest because these primarily show difference in the surface topography. Figure 2.8 show electron column component of SEM.

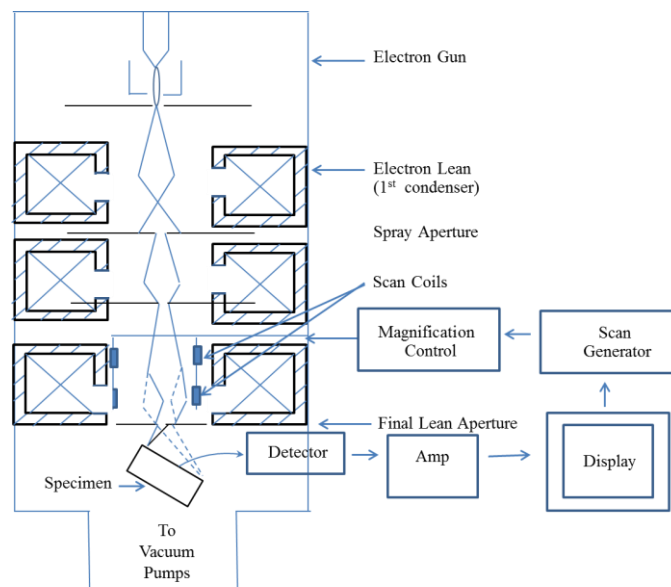


Figure 2.8 Schematic drawing SEM of the column showing electron gun, lenses the electron deflection, and electron detector.

2.2.3 Energy-dispersive X-ray spectrometer

Chemical analysis in the scanning electron microscope was performed by counting X-ray signal generated by electron beam interacting with matter. The principle of X-ray generations in the SEM specimen, the electron beam generated X-ray photon in the beam while interact with specimen surface. The EDS technique measures when X-rays as characteristic of the element was emitted from the sample during bombardment.

2.2.4 Raman spectroscopy

Raman spectroscopy is the characterization technique based on an inelastic scattering of a monochromatic excitation source. Raman is common vibrational spectroscopies similar with IR spectroscopy for assessing molecular motion and fingerprinting species. However, Raman spectroscopy was scattering technique that the scattering efficiency of detection depends on those molecules. In my work, Raman spectroscopy was used for observing the enhanced scattering efficiency of Au structures.

2.2.5 UV-visible spectroscopy

UV-visible spectroscopy is widely used for study of molecules and their electronic transitions of organic and inorganic material in solution phase. While light is traveling through the sample and transmitted light to detector, the characteristic of simple e.g., light absorption, is measured. The range UV-visible absorption directly affects the color of material. However, in case Ag and Au of metal nanomaterial show absorption and scattering in UV-visible range. In the UV-visible spectroscopy could be detected the optical property of metal nanomaterial by measuring absorbance spectrum which is the summation of absorption and scattering intensity of nanoparticles.

CHAPTER III

EXPERIMENTAL SECTION

3.1 Chemicals and materials

Sodium chloride (NaCl , $\geq 99.99\%$), nitric acid (HNO_3 , 65%), ammonia (NH_3 , 25%) and hydrochloric acid (HCl , 37% w/v) were purchased from Merck[®] (All chemicals were analytical grade and were used as received without an additional purification). De-ionized water was used as the solvent. Silver globules ($\geq 99.99\%$) and gold globules ($\geq 99.99\%$) with a diameter of 2-3 mm were purchased from a local precious metal retailer (UmniCore (Thailand)). A solution of gold (III) chloride (100,000 ppm/0.5 M Au^{3+}), AuCl_4^- , was prepared by dissolving 10 g of gold globules in aqua regia under a mild agitation and heating (80-100 °C). When all gold globules were completely dissolved after heating for at least 10 hours, the solution was further heated until almost dry. De-ionized water was added into the solution and adjusted volume to 100 mL. The gold (III) ion concentration was employed as a source of gold (III) ion for further investigation. {Caution: aqua regia, a mixture of HCl and HNO_3 with a volume ratio of 3:1, is very toxic chemicals and should be handled with care}. Prior to use, all glasswares were thoroughly cleaned with detergent, rinsed with de-ionized water, rinsed with aqua regia, and thoroughly rinsed with copious amounts of de-ionized water. Silver globules were ultrasonic cleaned before galvanic replacement.

3.2 Synthesis of coral-like gold nanostructures

The coral-like gold nanostructures on the surface of silver globules were prepared by galvanic replacement of silver metal (Ag^0) by gold (III) ion (Au^{3+}). Briefly, a few silver globules were immersed into a gold (III) ion solution under a continuous stirring. The 5,000 ppm (0.025 M) Au^{3+} solution was prepared by diluting 0.5 mL gold stock solution with 10 mL de-ionized water. After a 30 min immersion, the silver globules were removed from the solution and were cleaned with a copious amount of de-ionized water. The cleaned silver globule was further analyzed. The effect of gold (III) ion concentration on the coral-like gold nanostructures was

examined by performing the galvanic replacement reaction in 50, 100, 500, 1,000, 5,000 ppm gold (III) ion solutions (10 mL). The effect of pH gold solution was investigated by adjustable pH of gold (III) ion, pH 0 (without NaOH), pH 7, and 14, with NaOH (1 M) solution. The gold nanostructures development on the silver surface globules were examined after a 30min immersion. The time-dependent structural evolution of the corals-liked gold nanostructures was performed on a 5,000 ppm gold (III) ion solution (10 mL). The gold nanostructures developments on the silver surface were examined after 1, 5, 10, 20, 30, and 60 min immersion.

3.3 Synthesis of needle-liked gold nanostructures

The needle-liked gold nanostructures on the silver surface were prepared by galvanic replacement reaction between silver metal (Ag^0) and gold (III) ion under high concentration of chloride ion (Cl^-), in a typical experiment, silver globules were immersed into Au^{3+} (10 mL, 5,000 ppm) with 2 M NaCl. After 30 min immersion with a continuous stirring, the silver globules were removed and thoroughly cleaned under a flow of de-ionized water. The cleaned silver globule was further analyzed. The influences of the concentration of Cl^- on the NLGNs formation were examined by performing the reaction in a 5,000 ppm Au^{3+} solution with 0.1, 0.3, 0.5, 1.0, 2.0, and 3.0 M NaCl. The silver globules were immersed in the Au^{3+} solution with extra Cl^- for 30 min. The time dependent structural evolution of the NLGNs was performed on a system after 5, 10, 20, 30, and 60 min immersion time.

3.4 Ultrasonic assisted fabrication of coral-liked gold nanoporous

Free standing nanoporous gold was fabricated by galvanic replacement of a silver plate with Au^{3+} under an ultrasonic radiation. The ultrasonic radiation source was performed with ultrasonic cleaning bath. The 5,000 ppm of Au^{3+} (10 mL) solution was under an ultrasonic radiation, then silver plate with 0.5×0.5 mm diameter and 500 μm thicknesses were dropped into the solution. Silver plate was consumed and generated Au/AgCl composites within 10 min reaction time. Au/AgCl composites were removed from the solution and cleaned with a copious amount of de-ionized

water. The standing CLGPs were generated by dissolution of AgCl from gold structures using ammonia treatment method.

3.5 Dissolution of AgCl by ammonia treatment

The white AgCl salt, concomitantly developed along with the galvanized Au/AgCl composites, could be removed from the gold covered silver plate by immersion into ammonia solution (NH_3 , 10 mL, 10 % w/v) for 15 min. The residual ammonia was removed by rinsing with copious amount of water.

3.6 Characterizations

3.6.1 Scanning electron microscopy (SEM)

A galvanized silver globule was attached to a stainless steel stub through a carbon tape. Scanning electron microscopy micrographs were recorded with a JELO 6500A (analytical electron microscope) operated at 10-30 kV under high vacuum mode using a secondary electron imaging (SEI) and back scattering electron image (BSI). Elemental analysis was carried out using energy dispersive spectrometer (EDS) attached to the SEM.

3.6.2 X-ray diffraction (XRD)

Cleansed coral-liked and needle-liked gold film were performed using a Rigaku D/MAX-2200 instrument ($\text{Cu K}\alpha_1$ radiation) operated at 50 kV and 250 mA over range of 30 -90 by step scanning with a step size of 0.02.

3.6.3 Surface enhanced Raman scattering (SERS) measurement

The standing CLGPs were employed as SERS substrates while crystal violet (CV) and rhodamine 6G (R6G) used as a probe molecules. The silver globules after ammonia treatment was immersion into the solution with 0.01, 0.001, 0.0001 mM of probe molecule for 15 min. They were then immediately cleaned with copious amount of de-ionized water. The SERS acquisitions were performed on a room-temperature dried silver globules. A Raman microscope (DXR Raman, Thermo Scientific) was employed to record the SERS spectra. He-Ne laser at 532 nm was used as the excitation laser. A 10X long objective lens with a numerical aperture of

0.75 focused the excitation beam onto diameter of approximately 1 μm . The scattered light was collected using the same objective lens.

3.6.4 UV-visible spectroscopy (UV-vis)

5,000 ppm of AuCl_4^- solution diluted to 10 ppm with de-ionized water was used as a UV-visible sample. The quartz cuvette was cleaned by de-ionized water before collecting the spectrum. The sample was collected using a reference as pure distilled de-ionized water. USB 2000 spectrophotometer was a detector and light source using as Deuterium lamp (Bandwidth 200-850 nm).

CHAPTER IV

RESULTS AND DISCUSSION

4.1. Synthesis of coral-liked gold nanostructures

The color of silver globule rapidly changed from silver to dark blue within 30 min indicating a progress of galvanic reaction when an ultrasonic-cleaned silver globule was immersed into a 5,000 ppm of Au^{3+} solution. The orange-yellow color of the gold (III) ion solution was insignificantly changed although the color of silver globule was completely altered. An insignificant change in the UV/visible spectra was also observed. Figure 4.1 shows UV–visible absorption spectra of aqueous Au^{3+} solution before and after galvanic replacement reaction. The spectrum revealed a strong absorption band at 220 nm and a shoulder at 290 nm of Au^{3+} solution before galvanic replacement reaction, These bands were assigned as ligand-to-metal-charge-transfer (LMCT) transitions [61, 62]. The phenomenon indicates that the replacement reaction only occurs at the surface while minute amount of gold (III) ion was consumed by the reaction. The UV/visible spectra were dominated by the unreacted gold (III) ion complex showing that there was no silver ion (Ag^+) releasing into the solution. After prolong reaction time of 30 min, the solution was still clear while the UV/visible spectrum showed an undetectable change. These phenomena indicated that the galvanic generated AgCl was firmly attached on the surface of silver globules releasing of Ag^+ into the solution. AgCl was not released into the solution since there was no observable baseline shift after a prolong reaction time. The solution was still clear indicating that the galvanic-generated AgCl was attached no silver surface.

SEM micrographs of the galvanized silver globules (Figure 4.2) were in good agreement with the color change as the smooth surface of the silver globules was extensively damaged. A rougher surface could be noticed even from a low magnification image.

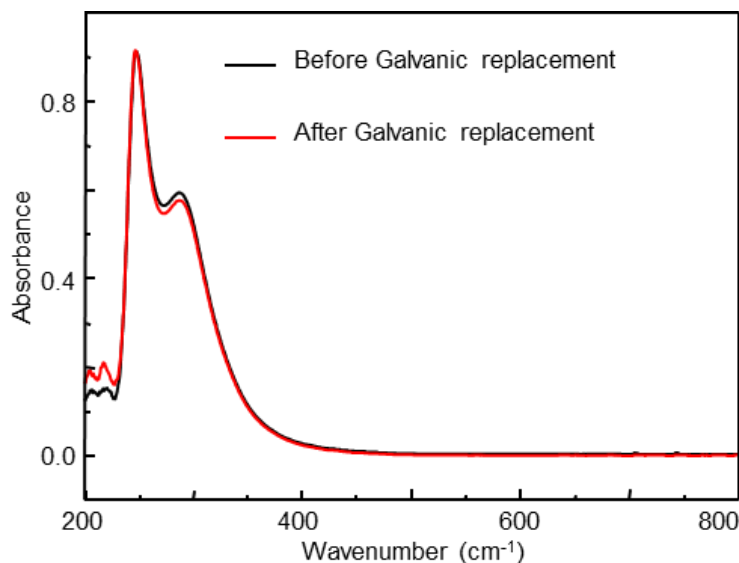


Figure 4.1 UV-visible spectra of 5,000 ppm Au^{3+} diluted to 10 ppm non reaction and 30 min galvanic replacement reaction.

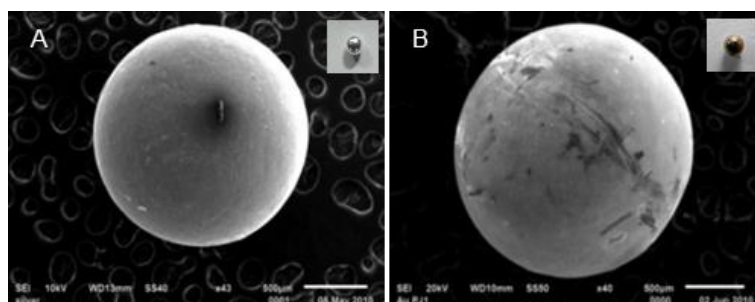


Figure 4.2 (A, B) Low magnification SEM micrographs of silver globules observed before and after galvanic replacement reaction 30 min, (inset) digital image of silver globules.

The elemental composition after 30 min galvanic replacement reaction was investigated by energy dispersive X-ray spectroscopy (EDS). Figure 4.3A EDS spectrum displayed strong peaks at 2.21, 2.62, and 2.98 keV which corresponding to Au, Ag, and Cl character. By following the ZAF method, the calculated elemental composition of Au/Ag/Cl ratio was about 14.67, 67.35, and 17.97 % atom. These results implied that galvanic replacement reaction generated solid AgCl formation co-deposited with Au atom [53]. The EDS spectrum (Figure 4.3B) shows high

intensity of Au and low intensity of Ag such that, 94.32 and 5.86 % atom after removing the AgCl solid with a NH_3 solution (ammonia treatment), while the signal for Cl was not detected. From the EDS data, it could be explained that the galvanic replacement reaction generated Au/AgCl composites and changed to pure Au structures after ammonia treatment. SEM micrographs (Figure 4.3A inset) showed the smooth morphology of AgCl patches with domain size of 1-2 μm covered with gold structures. Selectively dissolution of AgCl patches was performed by 10 % w/v NH_3 solution. Missing the large morphology of AgCl and the porosity of CLGNs with high surface roughness was appeared when AgCl was removed. The morphology of gold nanostructures is similar to a coral which called coral-like gold nanostructures.

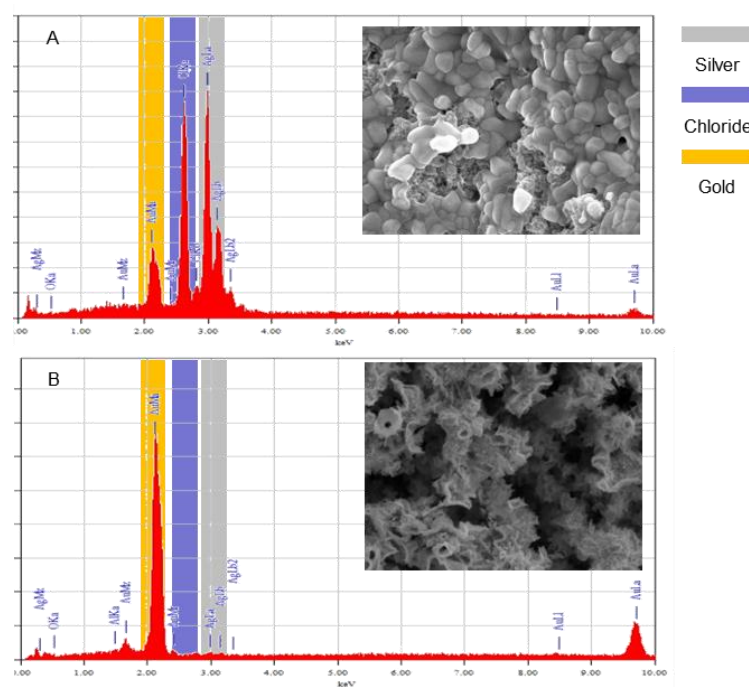


Figure 4.3 (A, B) Energy dispersive X-ray spectra of Au/AgCl layer with 30 min. before and after ammonia treatment, (inset) SEM micrographs of corresponding condition.

To confirm galvanic generated Au/AgCl composites by EDS mapping, the elemental distribution was displayed in Figure 4.4 showing Au, Ag, and Cl contents of Au/AgCl composites and CLGNs. Black and pink areas indicated low and high signal of those elements. The pink areas of Ag and Cl maps (Figure 4.4 A3, A4) are

more than that of Au map (Figure 4.4 A2) before AgCl removing. On the other hand, larger pink area of gold maps (Figure 4.4 B2) comparing with Ag and Cl was observed after AgCl removing.

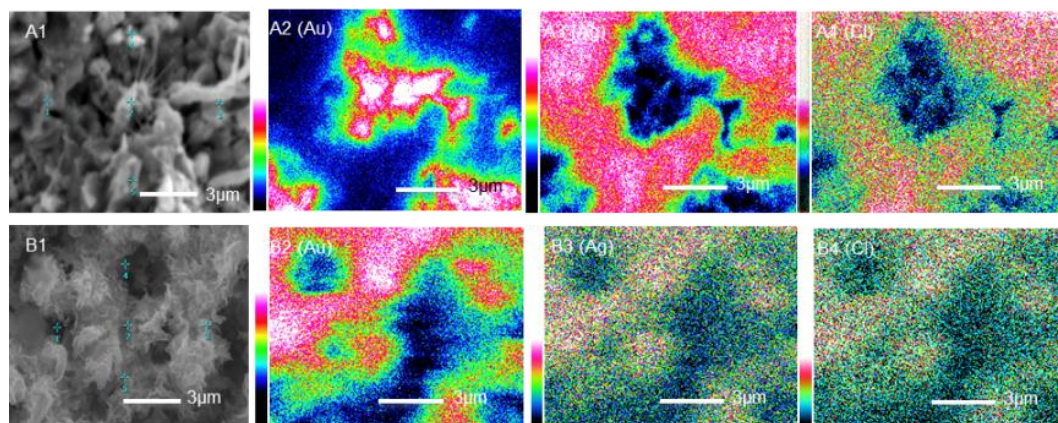


Figure 4.4 Elemental distributions at 30 min galvanic replacement reaction of silver globules and 5,000 ppm of Au^{3+} . (A1) SEM micrographs of galvanized silver globule surface before ammonia treatment, (A2-A4) Au, Ag, and Cl maps before ammonia treatment of silver surface. (B1-B4) corresponding SEM micrograph and EDS maps after remove AgCl by ammonia treatment.

The galvanic replacement reaction is one of the simple methods for creating complex structures (e.g., thin film, hollow structure, porous structure, bi metallic, and alloy) by consuming the more sacrificed metal component [63, 64]. When immersing silver metal into gold (III) ion solution, silver metal which acted as anode site was rapidly oxidized resulting Ag^+ and electrons (equation (5)). The electrons transfer to surface that acted as cathode site which captured Au^{3+} on silver surface generating Au^0 and Cl^- (equation (6)), while Cl^- reacted with Ag^+ and became AgCl (equation (7)). The solubility product (K_{sp}) of AgCl in water about 1.8×10^{-10} at 20°C due to solid AgCl co-deposited with gold [53, 65]. The size of AgCl patches is bigger than Au that controls Au deposition through AgCl layer, according to stoichiometry of AgCl which is 3 times more than Au. However, galvanic replacement reaction generated excess Cl^- into environmental reaction. The solubility of AgCl was decreased in the atmosphere of the excess Cl^- environment due to the common ion

effect as shown in equation (8) [65-67]. However ammonia treatment method was as a tool for studying the influential CLGNs formation as shown in Figure 4.6 as well as equation (9).

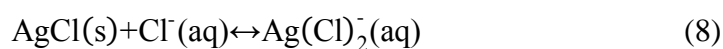
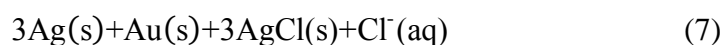
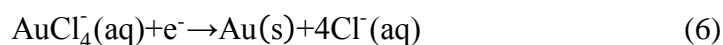
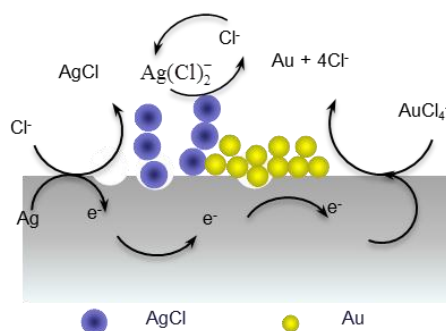


Figure 4.5 Schematic diagram of galvanic replacement reaction shows Au/AgCl co-depositions on sacrificed silver surface, *i.e.*, as the film become thicker. Equation (5, 6) oxidation and reduction reaction occurred as anode and cathode site. Equation (7) shows total galvanic replacement reaction. Common ion effects of AgCl are also depicted in equation (8).

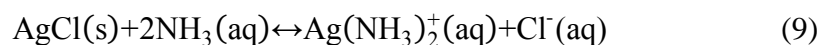
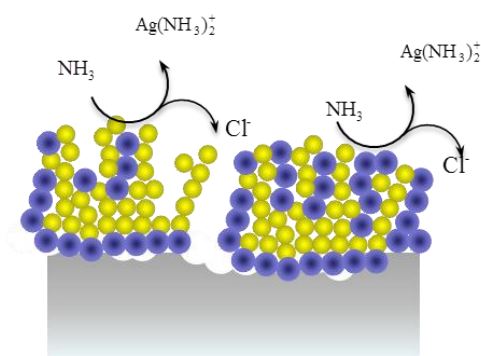


Figure 4.6 AgCl dissolution process by ammonia treatment (NH₃).

4.1.1. The concentration effect of Au^{3+} solutions on gold structures

Optical property of galvanized silver surface changes when increasing the concentration of Au^{3+} . Figures 4.7(A, B) show digital images of Au^{3+} solution at various concentrations (0, 50, 100, 500, 1,000, and 5,000 ppm) before immersing and immersing silver globules at 30 min of galvanic replacement reaction. At low concentrations, 50 and 100 ppm Au^{3+} , the yellow color did not appear while the light yellow was noticed at 500 ppm. The optical property of silver surface significantly changes when immersing silver globule at various Au^{3+} concentrations. At 50 and 100 ppm, the optical property of galvanized silver surface was not clearly changed. The galvanic reaction of low Au^{3+} concentrations and silver sacrificed layer was not change optical property of silver surface. Ultrathin film gold with 5nm was continuously deposited on substrate showing highly transparent property of gold film [68]. Light brown was appeared when increased concentration of Au^{3+} up to 500 ppm. The silver surface color was changed to black at high concentration, 1,000 and 5,000 ppm. Light brown and black result from the thinness of Au/AgCl composites was increased due to galvanic replacement reaction.

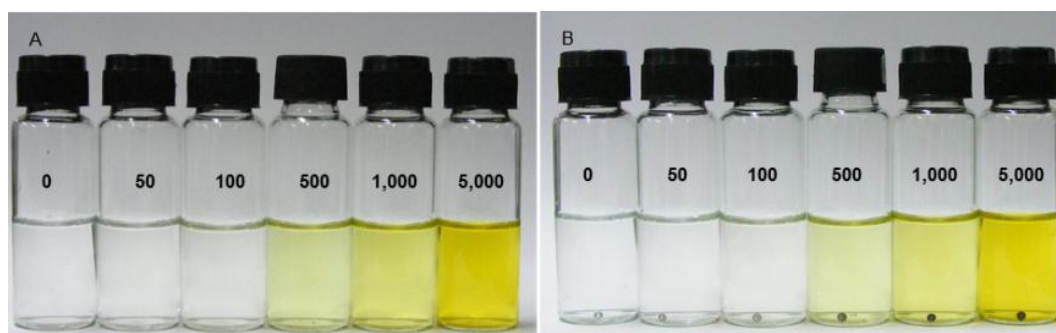


Figure 4.7 (A) Digital images of Au^{3+} concentration at 0, 50, 100, 500, 1,000, and 5,000 ppm. (B) Corresponding condition (A) of silver globule after 30 min of galvanic replacement reaction.

SEM micrographs were used to follow the structural evolution involving as various Au^{3+} concentrations. As the concentration of Au^{3+} increased from 50 ppm to 5,000 ppm, more complex Au structures were observed. At low concentration of Au^{3+} (Figure 4.8 A2, 50 ppm), spherical AgCl precipitated with domain size of 0.1-0.3 μm and scattered over the surface and aggregated to clusters

AgCl with domain size of 1.0-3.0 μm and were generated over the surface of silver surface. The clusters of AgCl precipitates grew larger once Au^{3+} was increased to 100 ppm (Figure 4.8 A3, 100 ppm). When the concentration of Au^{3+} was increased to 500 ppm (Figure 4.8 A4, 500 ppm), a plate-liked AgCl precipitates of smaller domain (1 μm) were generated. An even smaller plate-liked silver precipitation was obtained as the concentration of Au^{3+} was increased to 1,000 ppm (Figure 4.8 A5, 1,000 ppm). However, as the concentration of Au^{3+} was increased to 5,000 ppm (Figure 4.8 A6), larger plate-liked AgCl precipitations with smooth surface were obtained. The evidence of gold structures was observed in this condition by removing AgCl. After the removal of AgCl precipitates by ammonia treatment, the gold nanostructures were revealed. At low concentration of Au^{3+} (Figure 4.8 B2, 50 ppm), spherical gold nanoparticles with particle size of 80-400 nm were developed. Gold structures with plate-liked nanostructures start developing at 100 ppm of Au^{3+} concentration (Figure 4.8 B3). As the concentration of Au^{3+} increased (Figure 4.8 B4, 500 ppm), the gold plate with thickness size of 40-60 nm was grown in the direction normal to the silver surface. The plate length was increased when increasing concentration of Au^{3+} to 1,000 ppm (Figure 4.8 A5). As the concentration of Au^{3+} increased, larger and more delicate CLGNs were developed. The delicate CLGNs observed in Fig. 4.8 B6 suggest that the AgCl precipitates, which concomitantly generated with the gold structures, that prevented the collapse of the gold structures as the CLGNs grew inside the AgCl precipitates. Reaction rate of galvanic replacement depended on the concentrations of Au^{3+} [65]. The effect of Au^{3+} concentration on gold structures was confirmed by Nernst equation as shown in equation (6) [66]. Oxidation potential of galvanic replacement reaction depended on E_{cell} of reaction that related with concentration of Au^{3+} . Concentration of Au^{3+} was increased, deposition rate of Au atoms and AgCl were increased due to the oxidation potential of Au^{3+} . More complex gold structures were created with high concentration of Au^{3+} when prolonging reaction time.

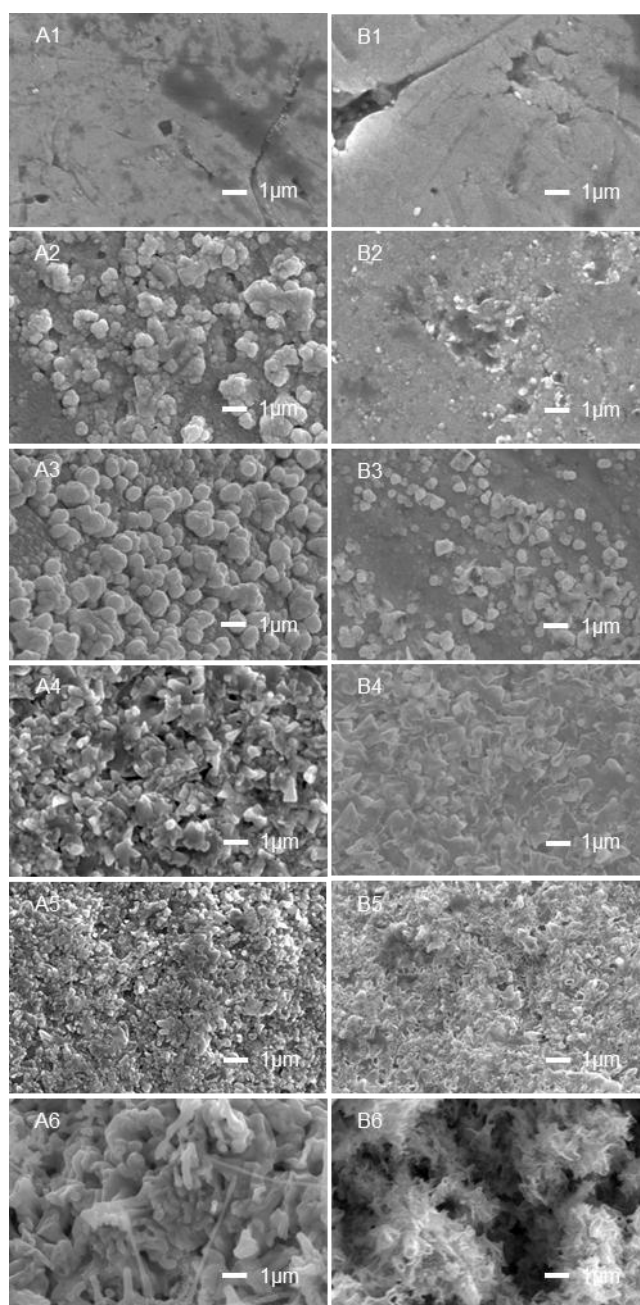


Figure 4.8 Structural developments of CLGNs due to concentration of Au^{3+} with 30 min reaction time. (A1-A6 and B1-B6) SEM micrographs of Au/AgCl composites and Au nanostructures increase the concentrations, 0, 50, 100, 500, 1,000, and 5,000 ppm Au^{3+} at 30 min of reaction time.

For an M^{n+}/M couple:
$$E = E^0 + \left(\frac{RT}{zF} \ln[M^{n+}] \right) \quad (6)$$

Where

- R = Molar gas constant = $8.314 \text{ JK}^{-1} \text{ mol}^{-1}$
- T = temperature in K
- Z = Number of moles electrons transferred per mole of reaction
- F = Faraday constant = 96485 Cmol^{-1}
- M^{n+} = Au^{3+} concentration in mol dm^{-3}

Elemental composition on galvanized silver surface with 50, 100, 500, 1,000, and 5,000 ppm of Au^{3+} was explored as shown in Figure 4.9. The atomic ratio of Ag/Au before ammonia treatment will be decreased when the Au^{3+} concentration increased from 50 to 500 ppm as 45.8, 13.80, and 3.70. Conversely, atomic ratio of Ag/Au was slightly changed when increasing the concentration of Au^{3+} up to 5,000 ppm, about 3.4, and 2.3. The atomic ratios of Ag/Au after ammonia treatment with any Au^{3+} concentration was decreased comparable before ammonia treatment. On the other hand, atomic ratio of Cl/Au before ammonia treatment insignificantly changed when increased the concentration of Au^{3+} to 5,000 ppm. But atomic ratio of Cl/Au at each concentration after ammonia treatment was decreased. Penetration depth of electron interaction with matter can be calculated from Kanaya and Okayama mathematical model that it could be explained differently atomic ratio of Ag and Cl with Au. Penetration depth of electron interaction with Au film about 857.32 nm was calculated with 20 keV by following equation (7) [69].

$$R_{\text{Au}}(\text{nm}) = 5.76E_0^{1.67} \quad (7)$$

Where

- R_{Au} = Bethe range, penetration depth (nm)
- E_0 = Beam energy (keV)

If the thinness of galvanized layer is lower than 857.32 nm, the signal of silver sacrificed layer was observed at 20 keV. In our case, monitoring of transformative gold thinness was traced by atomic ratio of Ag/Au. The galvanic reaction of Ag and low concentration of Au^{3+} (50 and 100 ppm) atomic ratio of Ag/Au is higher than high concentration of Au^{3+} (500, 1,000, and 5,000 ppm). Since Ag content was measured from silver sacrifice layer and AgCl from galvanized-layer. Electrons can pass through galvanized-layer to silver sacrificed layer, due to the thinness of galvanized layer is lower than electron penetration depth. Since the thinness of galvanized layer at high concentration of Au^{3+} is higher than electron penetration depth, only Ag signal from galvanized layer was detected. Atomic ratio Ag/Au was decreased because electron cannot interact with silver sacrificed layer. However the atomic ratio of AgCl is more than the standard molar ratio of Ag/Cl. X-ray photoelectron spectroscopy (XPS) and EDS results, the molar ratio of Ag/Cl was about 1.05 and 1.03 but both XPS and EDS can easily decompose AgCl into Ag [70].

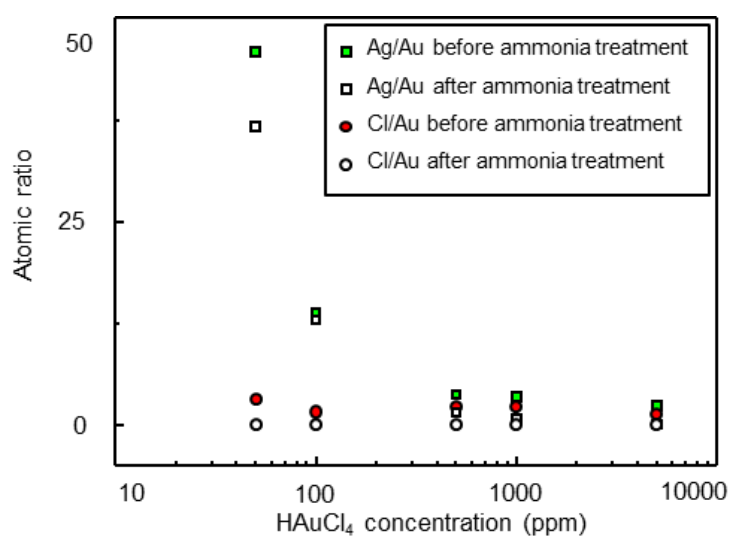


Figure 4.9 Elemental analysis of galvanized layer on silver surface with 0, 50, 100, 500, 1,000, and 5,000 ppm Au^{3+} solution at 30 min. (A) ratio of Ag/Cl (B, C) Au and Ag before and after ammonia treatment.

4.1.2. Time dependent evolution of CLGNs

Time dependent evolution of CLGNs at 5,000 ppm of Au^{3+} is followed by SEM. Figures 4.10 SEM micrographs of Au/AgCl and Au showed several

morphology of gold nanostructure before and after ammonia treatment that can be monitored structural growth by following reaction time, 1, 5, 10, 20, and 30 min. As 1 min of reaction time (Figure 4.10 A1), spherical AgCl precipitates with domain size of 60-100 nm dispersed over the surface as well as aggregated to clusters AgCl with domain size of 1-3 μm were generated over the surface of silver. The clusters of AgCl precipitates grew larger as reaction time was increased to 5 min (Figure 4.10 A2). When the reaction time was greater than 10 min (Figure 4.10 A3), semi-continuing AgCl layer were generated. Continuing AgCl layer were obtained as the reaction time was increased to 20 min (Figure 4.10 A4). However, when the reaction time was increased to 30 min (Figure 4.10 A5), AgCl dissolution phenomenon was observed with generating the gap of AgCl. At the same condition, micro-channels with domain size of 0.5-1 μm of silver chloride layer were obviously detected. The micro-channels inside AgCl structures resulted with Cl^- envelopment, these channels through AgCl are the main path for ionic transport [47]. Finally, NLGNs start to grow through AgCl structures at 30 min galvanized time. An evidence of CLGNs was observed in this condition by removing AgCl. Porous gold film with pore size of 50-800 nm was developed at 1 min of galvanic replacement reaction as shown in Figure 4.10 B1. That porous gold was produced from selective dissolution of AgCl without gold structures. Gold nanostructures with plate-liked nanostructures start developing on gold film since 1 min and more plate-liked nanostructures when increasing galvanized time to 5 min (Figure 4.10 B2). As the reaction time of the galvanic replacement reaction was increased to 10 min (Figure 4.10 B3), the plate-liked gold nanostructures with thickness size of 40-60 nm grew at normal direction and increased porosity of structures. Similarly growing as CLGNs was developed at 20 min (Figure 4.10 B4). The complexity of CLGNs was increased when increasing galvanized time to 30 min (Figure 4.10 B5), while NLGNs start developing on plate-liked gold nanostructures at this condition. At 60 min of galvanic replacement reaction increased, a larger and more delicate CLGNs and NLGNs were developed. The delicate CLGNs observed in Figure 4.10 B6 suggested that the AgCl precipitate, which concomitantly generated with the gold structures, prevented the collapse of the gold nanostructures as the CLGNs grew inside the AgCl precipitates. Time dependent evolution of CLGNs development was confirmed by following the history of galvanized layer growth. The

vertical panorama SEM micrograph was the new technique for characterization the detail of gold film layer. Figure 4.10 (C), cross section vertical panorama SEM micrograph with thickness 22 μm on CLGNs was captured at 30 min reaction time. The galvanized layer at initial state, dense gold was epitaxial depositing with layer thickness about 300 nm. The dense gold layer resulting epitaxial deposition of Au on silver surface was attached more than AgCl. This can be caused by the same lattice constants of gold (0.408) and silver (0.409), While the lattice constant of silver chloride (0.544) was different due to AgCl no epitaxial depositing on gold and silver [71]. The gold nanoporous clearly developed when the galvanized layer grew up to 500 nm. Gold nanoporous with 50-80 nm was observed at 500-5,000 ppm of Au^{3+} solution. Larger AgCl precipitate was formed as the thickness of galvanized layer increasing since 2 μm up to completely layer. That occurrence can be noticed from micro porous on CLGNs layer. The grain defect of AgCl and Au on Au/AgCl composites was appear due to different lattice constants.

4.1.3. AgCl under layer formation on the Au/AgCl composites

Figure 4.11 showed the SEM micrographs of CLGNs observed AgCl under layer formation phenomena. Cross-section of CLGNs at 5, 30, and 60 min before and after galvanic reaction were separated from Ag sacrificed surface. At 5 sec of galvanic replacement reaction, spherical gold with domain of 150-300 nm grew on sacrificed silver surface with thickness of 700-800 nm while the grain boundary of Ag indicated on the silver surface due to galvanic corrosion. After ammonia treatment the morphology and thickness of CLGNs is similar with that before ammonia treatment. The results confirmed epitaxial deposition of Au on silver surface and no epitaxial deposition of AgCl on Ag surface. Au atoms could be deposited on silver surface is more than AgCl, morphology of Au/AgCl nanocomposites after ammonia treatment was no observed. AgCl under layer formation was observed at 30 sec of galvanic reaction. The thickness of Au/AgCl composite before ammonia treatment about 1.6 μm was decreased to 1.2 μm after ammonia treatment. Then AgCl was detected on silver surface but porous structures on silver surface were noticed after ammonia treatment. The corrosive silver surface occurred while galvanic reaction was implied due to AgCl formation under layer. When prolonging the reaction, AgCl under layer was

clearly generated between Au/AgCl composites and silver surface. The thinness of Au/AgCl composite and AgCl under layer about 2.6-3 μm before ammonia treatment was decreased to 1.9-2.3 μm after ammonia treatment.

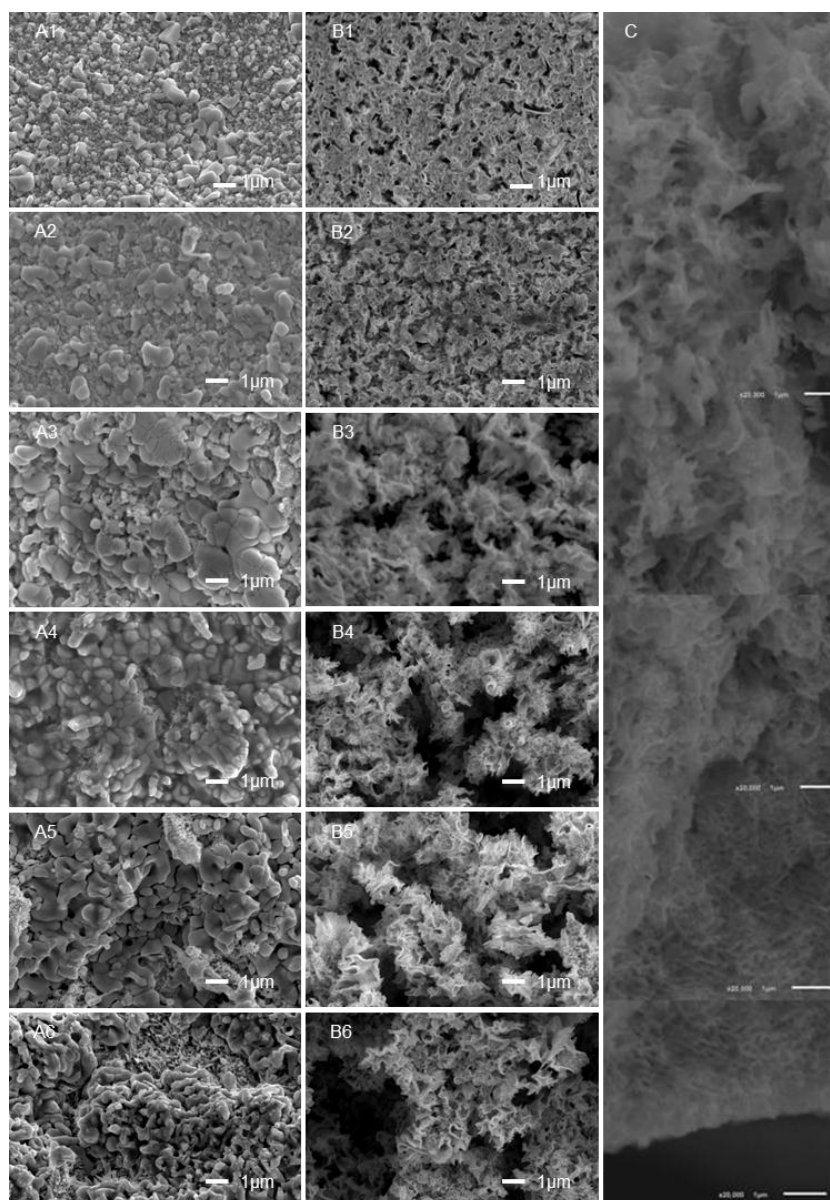


Figure 4.10 (A1-A6) Time dependent evolution of Au/AgCl co-deposited on silver globules surface by galvanic replacement reaction, silver globules and 5,000 ppm Au^{3+} at 1, 5, 10, 20, 30, and 60 min respectively, (B2-B6) structural development of gold after removing silver chloride by ammonia treatment. (C) Cross section vertical panorama SEM micrograph on CLGNs with 30 min reaction time.

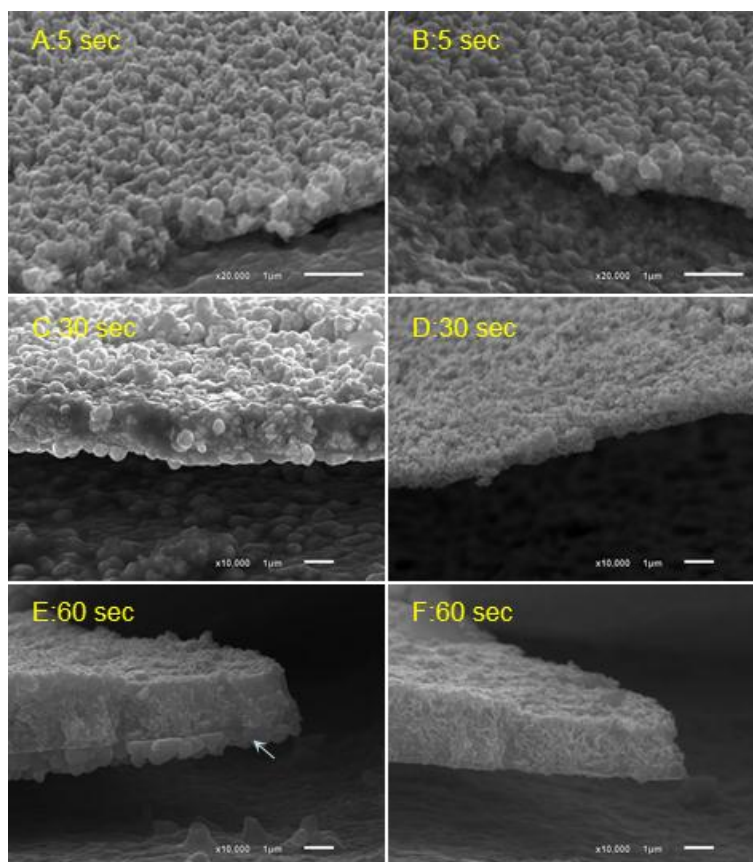


Figure 4.11 (A, C, and E) SEM micrographs of cross section galvanized silver surface with 5,000 ppm Au^{3+} at 5, 30, and 60 sec reaction time before ammonia treatment.

4.1.4. The pH of Au^{3+} solution influence on gold structures

Generally, highly acidic condition (pH 0) of Au^{3+} solution was prepared by dissolving Au metal with aqua regia. At neutral (pH 7) and alkaline (pH 14) conditions were tuned by adjusting with NaOH. The pH effects of Au^{3+} solution on galvanic replacement reaction were depicted in Figure 4.12. The optical property changed from silver to dark brown, light brown and muddy silver when increasing NaOH. The effects of pH on gold structures transformation were confirmed by SEM micrographs. SEM micrographs showed the complexity of the galvanized silver surface was decreased when increasing pH of Au^{3+} at the acidic to alkaline conditions. SEM micrographs of galvanized silver surface indicated the normal condition of galvanic replacement reaction after ammonia treatment. Gold prefer to grow on silver

surface as a CLGNs with plate thickness of 80-100 nm. At neutral condition of Au^{3+} , Zen stone-like gold microstructures with diameter of 10-12 μm was developed as vertical direction. When the pH of Au^{3+} solution was adjusted to alkaline condition (pH 14), the AgCl precipitates was appeared due to insignificant change on galvanized silver surface (Figure 4.12 C).

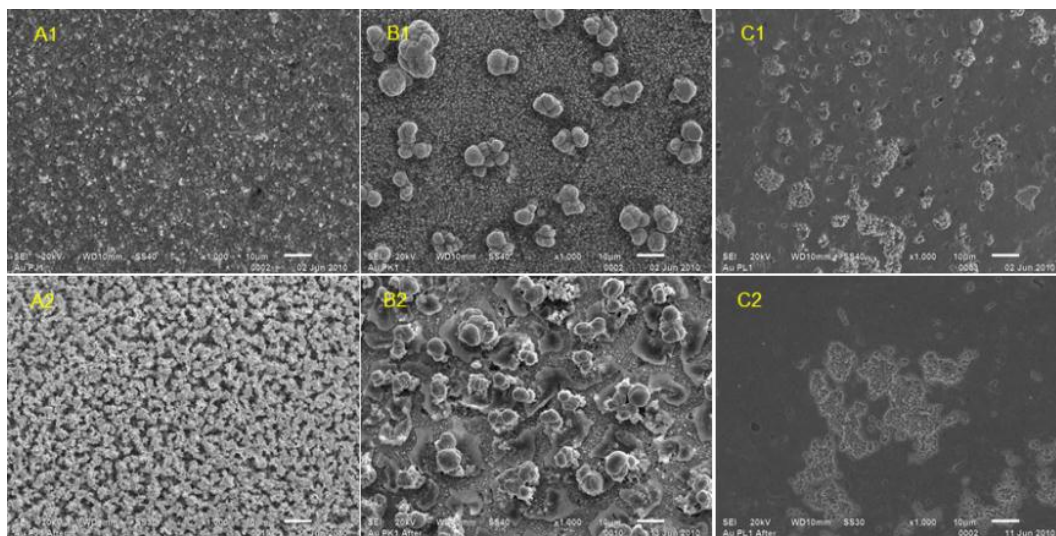


Figure 4.12 Structural developments of coral-like, Zen stone-like gold nanostructures, and gold thin film due to pH of Au^{3+} solution with 30 min reaction time. (A, B, and C) SEM micrographs of galvanized silver surface of 5,000 ppm of Au^{3+} solution with pH 0, 7, and 14, reaction time 30 min respectively. (1 and 2) SEM micrographs were compared after ammonia treatment.

To observe the elemental composition of galvanized layer at vary pH (7, and 14) by EDS was compared with normal condition (pH= 0). Figure 4.12 shows atomic ratios of galvanized layer at pH 0, 7, and 14 (A, B) before and after ammonia treatment. Atomic ratios of Ag/Au and Cl/Au had good results of 2.33 and 1.43 at pH 0 of Au^{3+} solution. When the pH of Au^{3+} was increased up to neutral, atomic ratios of Ag/Au and Cl/Au was insignificantly decreased to 1.49 and 1.21 although the Zen stone-like gold microstructures completely changed. However the galvanic replacement reaction Au^{3+} at alkaline condition with Ag metal, atomic ratios of Ag/Au and Cl/Au is more than previous conditions. After ammonia treatment, atomic

ratio of Ag/Au was upturn to 108.3 while atomic ratios of Cl/Au dropping to 0.58. However atomic ratios of Ag/Au and Cl/Au at neutral condition are similar to that of acidic condition after ammonia treatment. The EDS mapping of Zen stone-like gold microstructures clearly indicated in Figure 4.13.

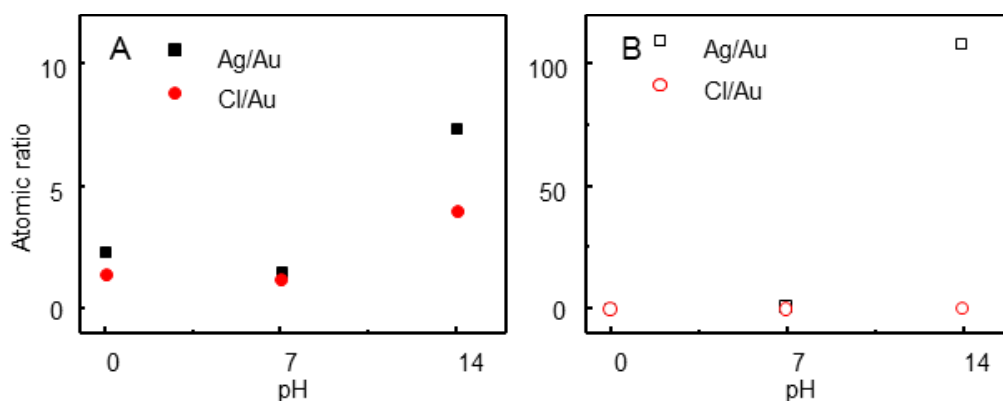


Figure 4.13 Atomic ratios of Ag/Au and Cl/Au on galvanized-layer at pH 0, 7, and 14 (A, B) before and after ammonia treatment.

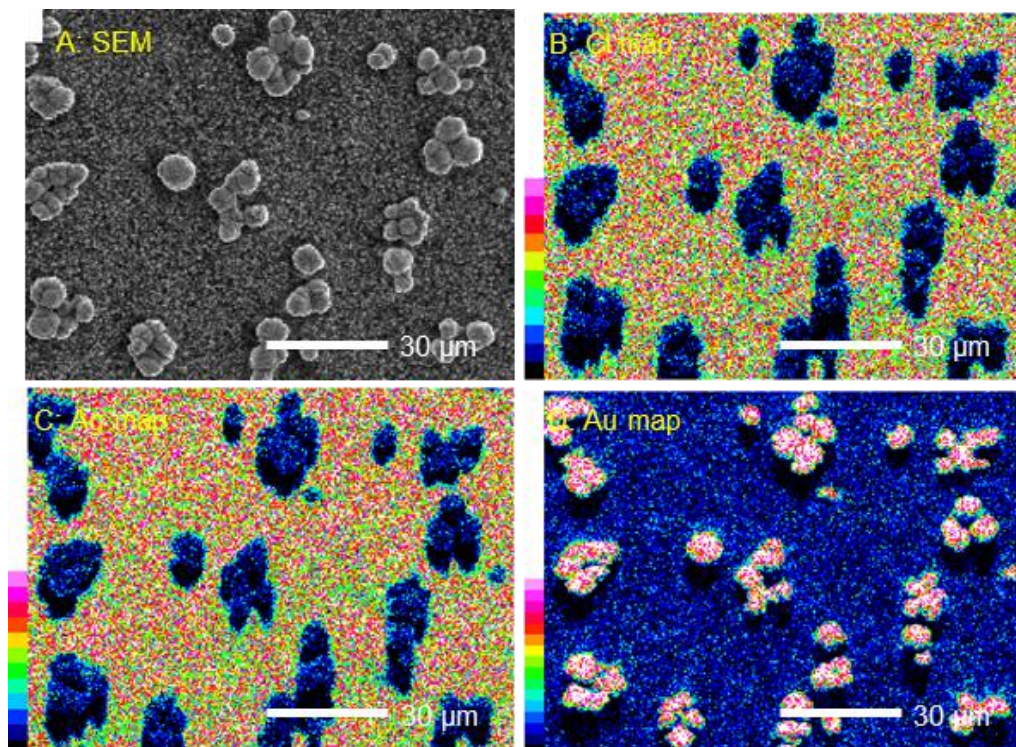


Figure 4.14 EDS mapping of elemental Zen stone like-gold microstructures (A) SEM micrograph, (B, C, and D) Cl, Ag, and Au mapping.

4.2. Synthesis of NLGNs

Figure 4.14 shows NLGNs using the same chemical as that of CLGNs synthesis. Low magnification SEM micrographs of the complete galvanized layer before and after ammonia treatment are shown in Figure 4.14 (A, B), it is noticeable that the structural changing on the top surface of NLGNs was not observed. Unchangeable NLGNs was implied that the needle structures completely coverage AgCl. The cross-section view of SEM micrographs with back scattering detector was shown in Figure 4.14 (C, D). A white and brown area refers to Au and AgCl that showing NLGNs grew through AgCl structures. Figure 4.14 (E) corresponds to the previous Figure captured with secondary electron detector (SEI) as normal SEM micrographs.

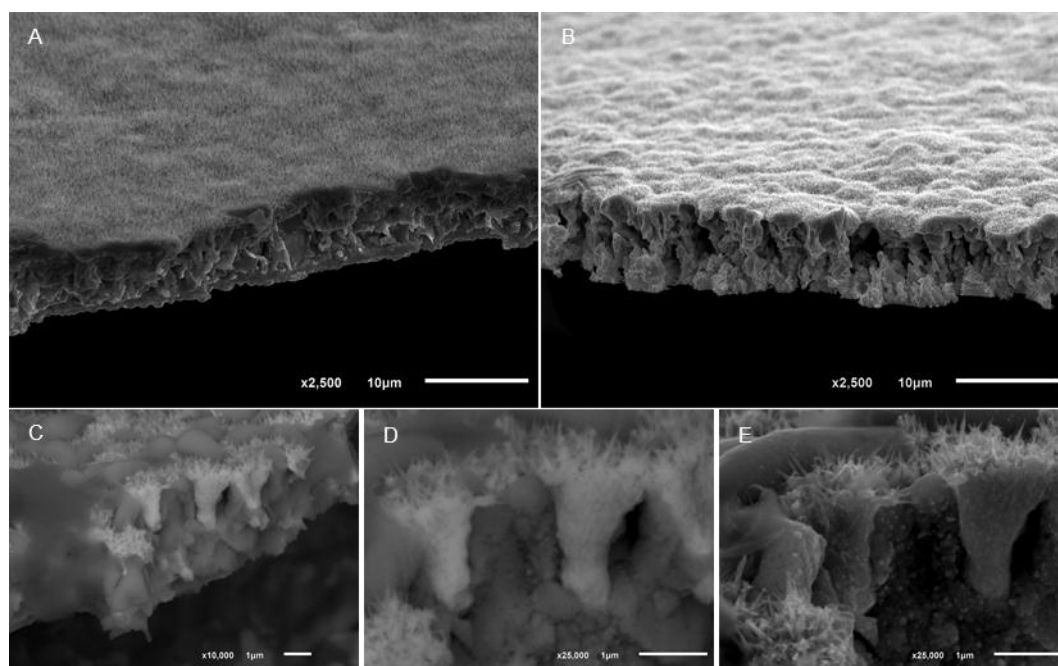


Figure 4.15 (A, B) SEM micrographs of NLGNs before and ammonia treatment (C, D) SEM micrographs with back scattering detector (E) corresponding SEM micrograph with (D).

4.2.1. The effect of NaCl on NLGNs

The NLGNs with single tip was growing with the same condition as that of CLGNs. Silver metal was dipped into 5,000 ppm Au^{3+} with 2 M NaCl, the

NLGNs occurred. Cl^- is key factor of NLGNs growth. When 5,000 ppm Au^{3+} mixed with 2 M NaCl, light yellow no change while silver globules performing the slow change of color to black when galvanic replacement occurred. The different NaCl concentrations (0 M, 0.1M, 0.5 M, 1M, 2M, 4M NaCl) mixing with 5,000 ppm Au^{3+} was monitored at 30 min reaction time as shown in Figure 4.15. The galvanic replacement reaction without adding NaCl, CLGNs was obtained. At 0.1 M NaCl mixing with 5,000 ppm Au^{3+} , thorn-liked gold nanostructures with diameter of 100-500 nm and the length of 1-2 μm was developed blending with AgCl as smooth surface. These structures distinctly noticed after removing AgCl. Larger diameter and the length of thorn-liked gold nanostructures developed over AgCl structure when increasing to 0.3 M NaCl. At the same condition of initial state of NLGNs with tips diameter of 80-120 nm and needle length of 1-1.3 μm joined with thorn-liked gold nanostructures. At the concentration of NaCl was increased to 0.5M, the NLGNs with smaller tip grew longer into vertical direction. Only NLGNs developed on the gold film when increasing NaCl until 3 M NaCl. However, connecting NLGNs layer was not completely covered the total area of silver sacrificed surface.

4.2.2. Micro-channel on AgCl layer

In previous experiment, ammonia treatment was applied for detecting structural transformations of galvanized layer including Au/AgCl composites and Au structures without AgCl precipitates. In this experiment, the ammonia treatment was used to study the middle AgCl layer, 0.5 % w/v NH_3 softly dissolved AgCl on the surface galvanized layer for 15 min. All NLGNs were synthesized using 5,000 ppm Au^{3+} with 2 M NaCl as 30 min of galvanic replacement reaction. Figure 4.17, SEM micrographs show galvanized surface which was removed AgCl at 0, 0.5, and 10 % w/v NH_3 . Micro channel with diameter of 300-500 nm was detected on AgCl surface, original NLGNs was fabricated as shown in Figure 4.17 A. When using low concentration of NH_3 , AgCl was not completely removed. The residue of AgCl layer showed in Figure 4.17 (B), the micro channels only occurred on AgCl layer. This phenomenon was confirmed that the gold surface insignificant detected micro channel. However AgCl was completely dissolved by using 10 % w/v which the micro channel cannot observe.

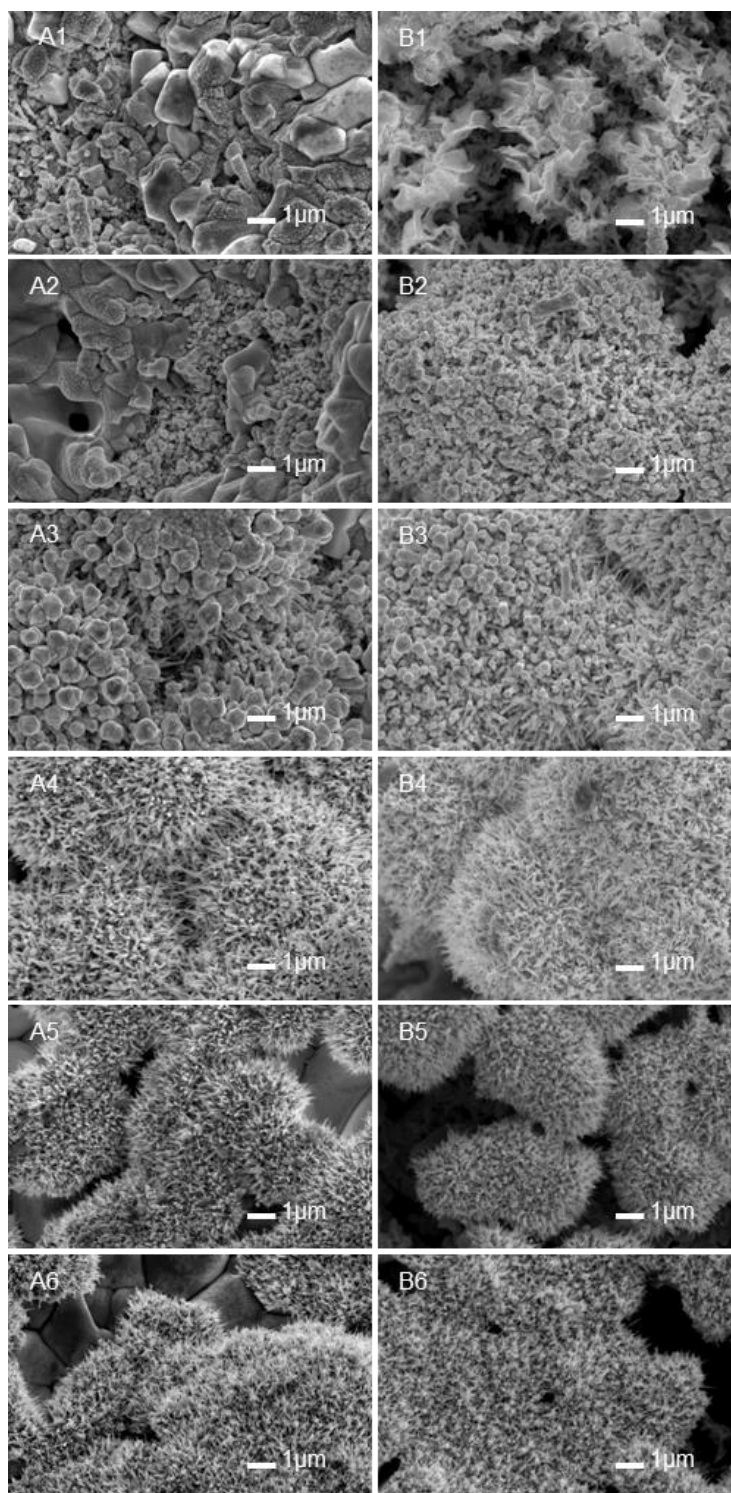


Figure 4.16 (A1-A6) Structural developments of NLGNs by galvanic replacement reaction, silver globules and 5,000 ppm of Au^{3+} solution was mixed 0, 0.1, 0.3, 0.5, 1, 2 M NaCl at 30 min respectively. (A2-A6) structure developments of NLGNs after remove AgCl by ammonia treatment.

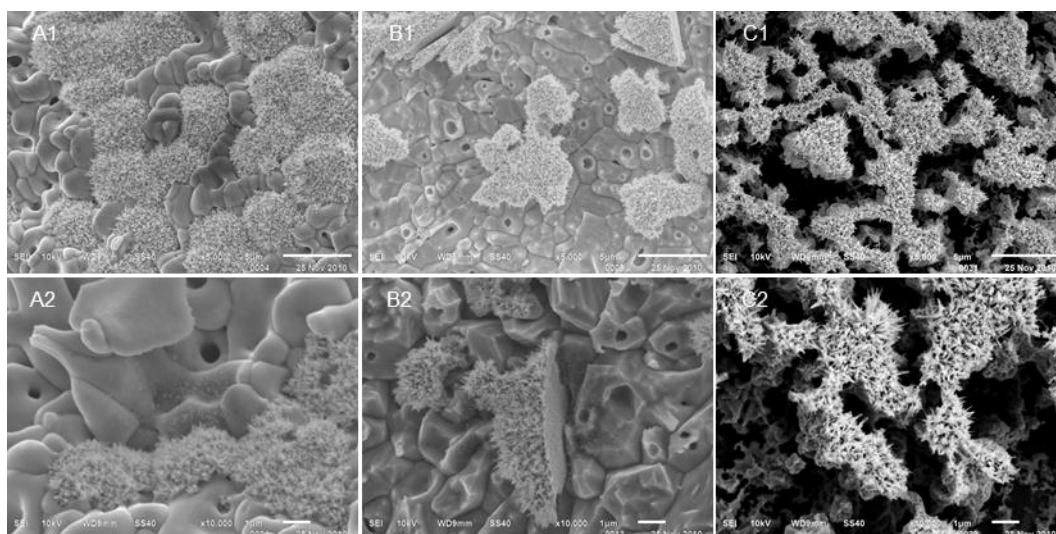


Figure 4.17 (A, B, and C) SEM micrographs of galvanized silver was removed AgCl with 0, 0.5, and 10 % w/v NH_3 . (1 and 2) SEM magnifications take with 5,000x and 10,000x

4.2.3. Time dependent evolution of NLGNs

Structural evolution of NLGNs due to reaction time of galvanic replacement reaction was monitored by SEM. From Figures 4.17, SEM micrographs of galvanized layer were observed the growth mechanism steps of NLGNs by monitoring the reaction time as follows: 0, 5, 10, 20, and 30 min. Figure 4.17 A1, SEM micrographs of silver sacrificed surface before galvanic replacement reaction has taken place with insignificant changed after ammonia treatment. After 5 min galvanic replacement reaction, AgCl concomitant with domain size of 1-1.5 μm grew over gold structures. The micro porous gold with domain size of 1-1.5 μm was observed after removing AgCl. The differential structures comparable to similarly condition of CLGNs, the plate-like gold nanostructures cannot develop on gold film at 5 min reaction time. When the reaction time increased to 10 min (Figure 4.17 A3), gold cluster with domain size of 5-6 μm were generated through AgCl layer. Little plate-like gold nanostructures were developed on the gold cluster and no AgCl feature co-deposited on gold cluster. Continuous galvanic replacement reaction occurred as the reaction time increased to 20 min (Figure 4.14 A4). Selective

deposition of gold due to galvanic reaction was filled on gold cluster, little plate-like gold nanostructures transformed to NLGNs.

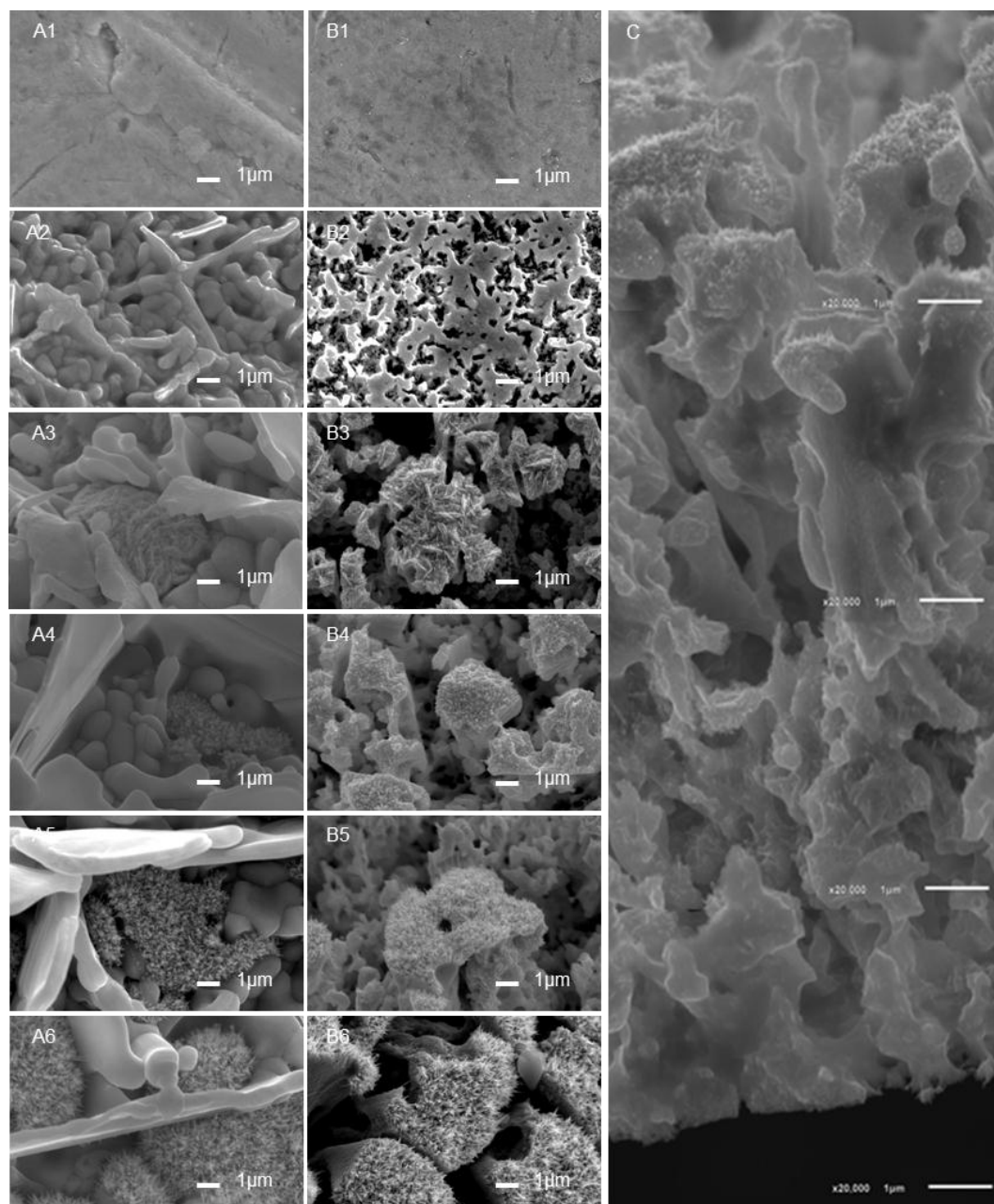


Figure 4.18 (A1-A6) Time dependent of NLGNs by galvanic replacement reaction between silver globules and 5,000 ppm Au^{3+} was mixed 2 M NaCl at 0, 5, 10, 20, 30 and 60 min respectively. (A2-A6) corresponding of NLGNs after removing AgCl by ammonia treatment.

When the reaction time increased to 30 and 60 min (Figure 4.14 A5, A6), finally NLGNs was generated on gold cluster. The vertical panorama SEM micrograph shows the detail growth of NLGNs. Cross section vertical panorama SEM micrograph with thickness of 13-15 μm on NLGNs was captured at 30 min reaction time. The galvanized layer at initial state, dense gold was epitaxial depositing with continuous layer.

4.2.4. X-ray diffraction (XRD) pattern of the CLGNs and NLGNs

Figure 4.20 shows X-ray diffraction (XRD) pattern of the CLGNs and NLGNs after ammonia treatment. The XRD pattern obtained four peaks at 38.12, 44.12, 64.48, 77.5 corresponding to the (111), (200), (220), (311) planes of a face centered cubic lattice [17, 18]. It is worth noting that the intensity ratio (coral 0.42), needle 0.37) of the 200 to 111 that one is lower than the conventional intensity ratio (gold powder 0.52) [19, 20]. These observations imply that the deposited of CLGNs and NLGNS tend to nucleate and grow into their surfaces terminated by the lowest energy (111) facets

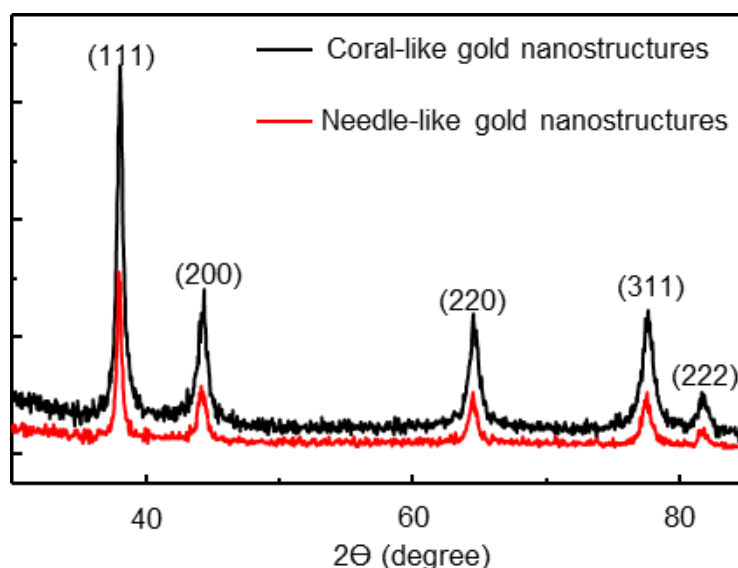


Figure 4.19 XRD patterns of CLGNs and NLGNs after ammonia treatment

4.3. Synthesis of standing coral-liked gold nanoporous

The standing CLGPs synthesis by using ultrasonic assisted. (1) The advantage of the method, fast galvanic creation complex nanostructures, (2) no additive agent such as capping agent, stabilizer, reducing agent, and (3) easy cleaning. Fabrication of CLGPs as microstructures using ultrasonic radiation was assisted at room condition.

4.3.1. Optical property of Au/AgCl composites

Figure 4.22 shows digital image as a video snap shot of galvanic reaction (A) 5,000 ppm of Au^{3+} before galvanic replacement reaction, (B-E) galvanic replacement reaction at 00:00.000, 00:0.083, 00:09.167, 00:20.242, and 07:13.917 reaction time (sec). The fast galvanic replacement reaction created Au/AgCl composites at 0.83 sec, the color of silver surface change to black (Figure 4.22 (B compares with C)). Au/AgCl composites were ejected from silver surface when the reactions continuously occurred to 9.16 sec. the clearly phenomena was observed at 20 sec, the black diffused to Au^{3+} solution while silver color appeared on silver surface. Au/AgCl composites were released under ultrasonic radiation condition due to regenerate Ag free surface. Regenerative free Ag surface and galvanic replacement reaction occurred as circle galvanic replacement reaction and completely consumed Ag sacrifice at 7-10 min.

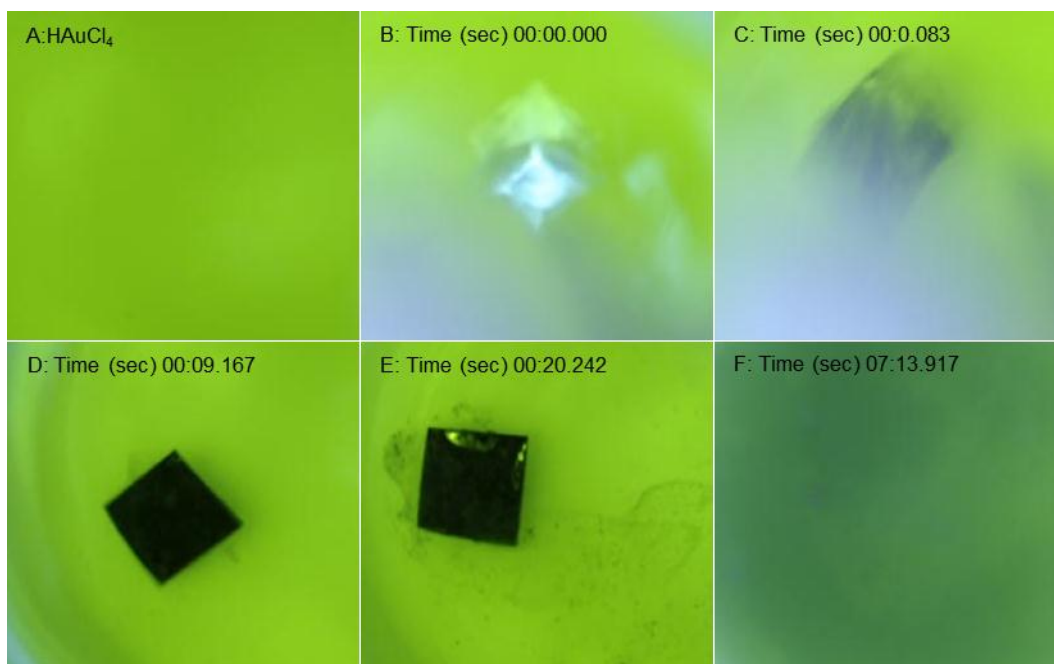


Figure 4.20 Digital images of snap shot video of galvanic reaction (A) 5,000 ppm Au^{3+} before galvanic replacement reaction (B-E) galvanic replacement reaction at 00:00.000, 00:0.083, 00:09.167, 00:20.242, and 07:13.917 reaction time (sec).

4.3.2. UV-visible change of Au^{3+} solution on galvanic replacement reaction

Optical absorption of Au^{3+} before and after galvanic replacement reaction was investigated by UV-visible spectroscopy. The Figure 4.23 shows UV-visible absorption spectra of aqueous Au^{3+} solution before and after galvanic replacement reaction. The strong adsorption band at 220 nm and shoulder at 290 nm were decreased when galvanic replacement reaction completely consumed Ag. The orange-yellow color of the gold (III) ion solution was insignificantly changed to green after galvanic replacement reaction. Figure 4.23 (A, B) inset image shows the color of Au^{3+} solution before and after galvanic reaction.

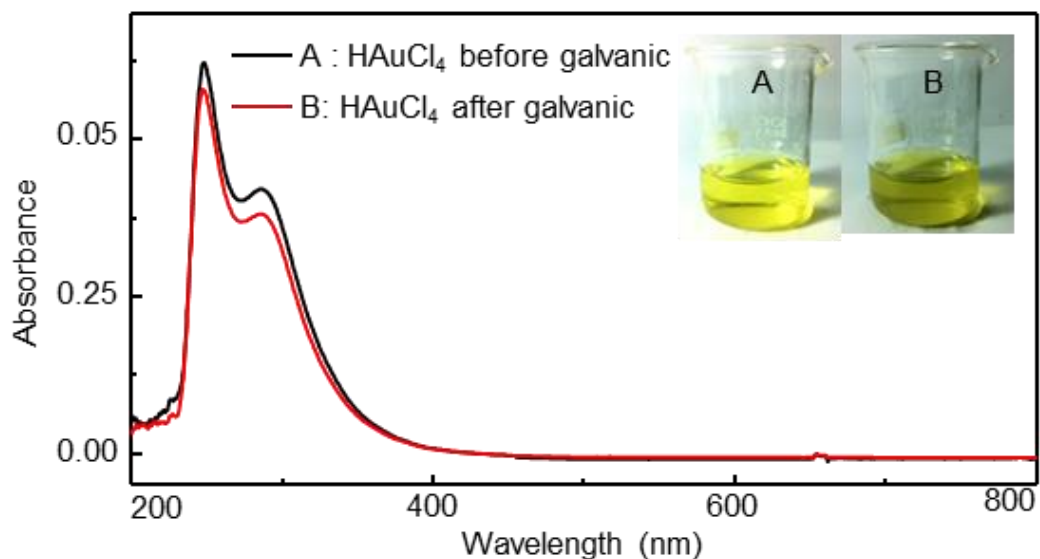


Figure 4.21 (A, B) UV-visible spectra of 5,000 ppm Au^{3+} diluted to 10 ppm before and after galvanic replacement reaction. Image inset: Digital image of Au^{3+} solution.

4.3.3. The morphology of CLGPs

SEM micrographs of Au/AgCl composites and CLGPs after removing AgCl show in Figure 4.24. Au/AgCl composites with domain size of 80-300 nm at upper layer was formed Au/AgCl micro plates with a thinness of 1-2 μm . A continuous layer of AgCl part with domain size of 0.3-1 μm was investigated lower of Au/AgCl composites. CLGPs were generated when AgCl was removed under NH_3 condition. Pore size of CLGPs was the combination of between nano and micropores. Pore size of micropores about 150-300 nm was produced on the surface of CLGPs and pore size of nanopore about 30-60 nm was investigated inside of micropores. Figure 4.25 shows pore size distribution of CLGPs. Inset Figure 4.25 was the SEM micrograph which was captured at high magnification (100,000X) of CLGPs.

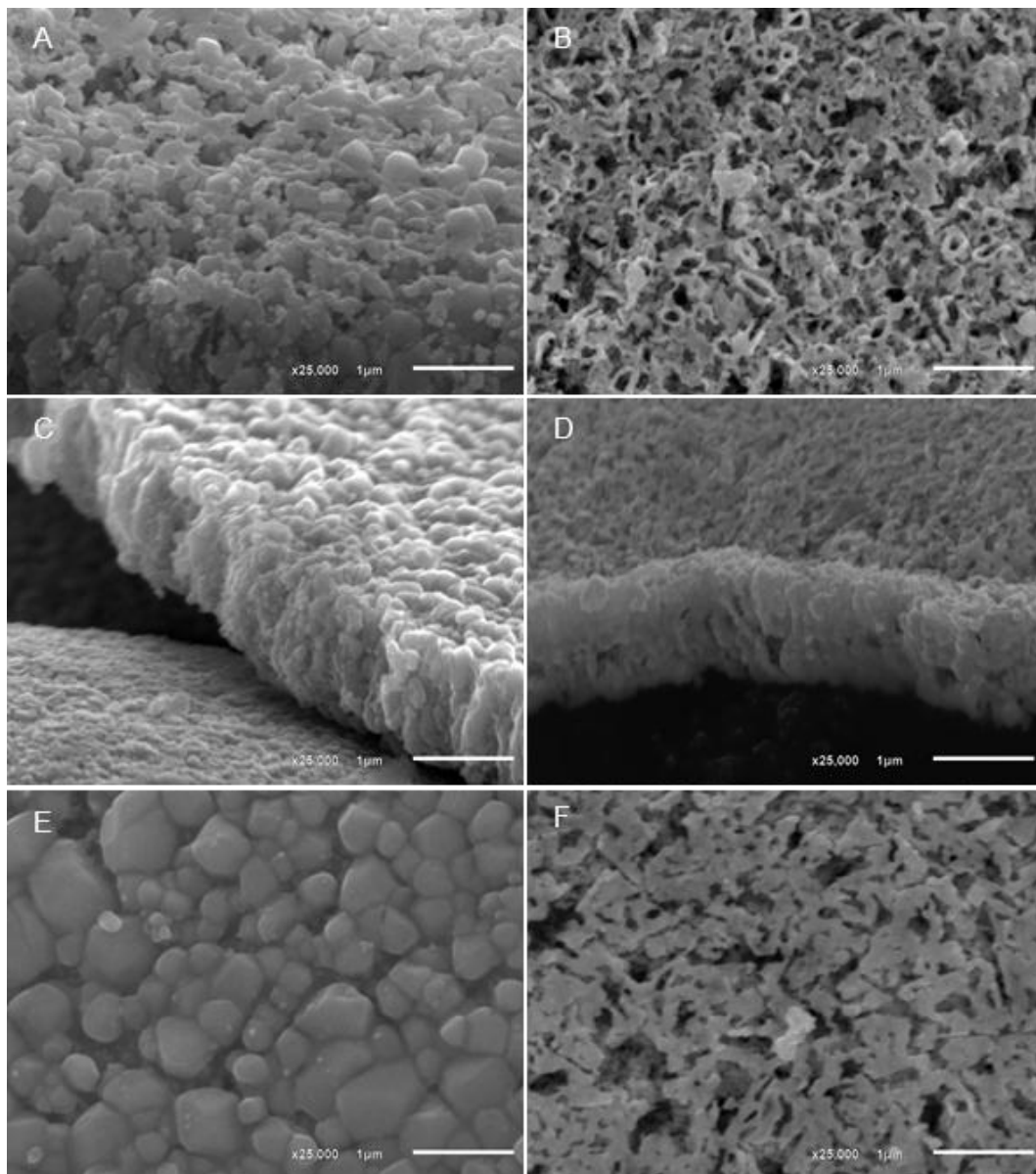


Figure 4.22 CLGPs synthesis by using ultrasonic assisted, (A, C, and E) SEM micrographs CLGPs before ammonia treatment and (B, D, and F) after galvanic replacement reaction.

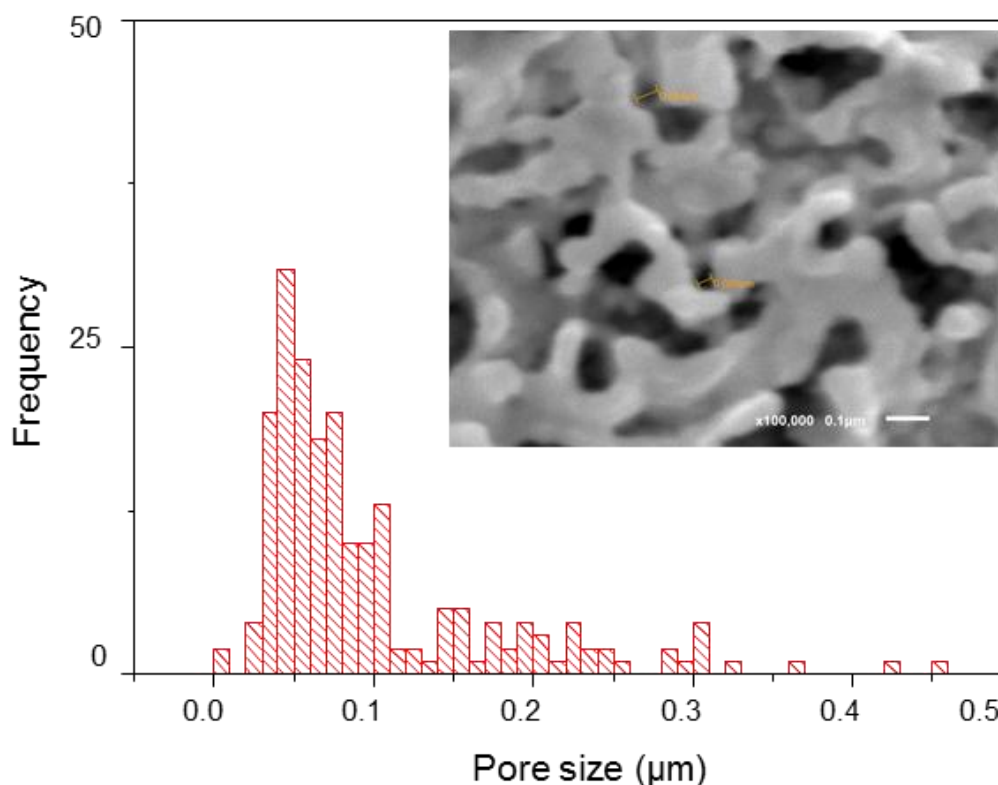


Figure 4.23 Pore size distribution of CLGPs show combinations of micro and nanoporous on structures, (inset) SEM micrograph captured with high resolution.

4.3.4. Elemental composition of Au/AgCl composites and CLGPs

The elemental composition of Au/AgCl composites and CLGPs were shown in Figure 4.25. EDS spectrum showed high intensity of Au, Ag, and Cl at 2.21, 2.621, and 2.983 keV, the atomic ratio of Au/Ag/Cl is about 19.86, 44.96, 35.17. After removing AgCl by ammonia treatment, atomic ratio of Au was strongly increased to 96.27 while Ag and Cl about 3.74 and 0 were detected. The morphology of CLGPs included Ag inside gold structure.

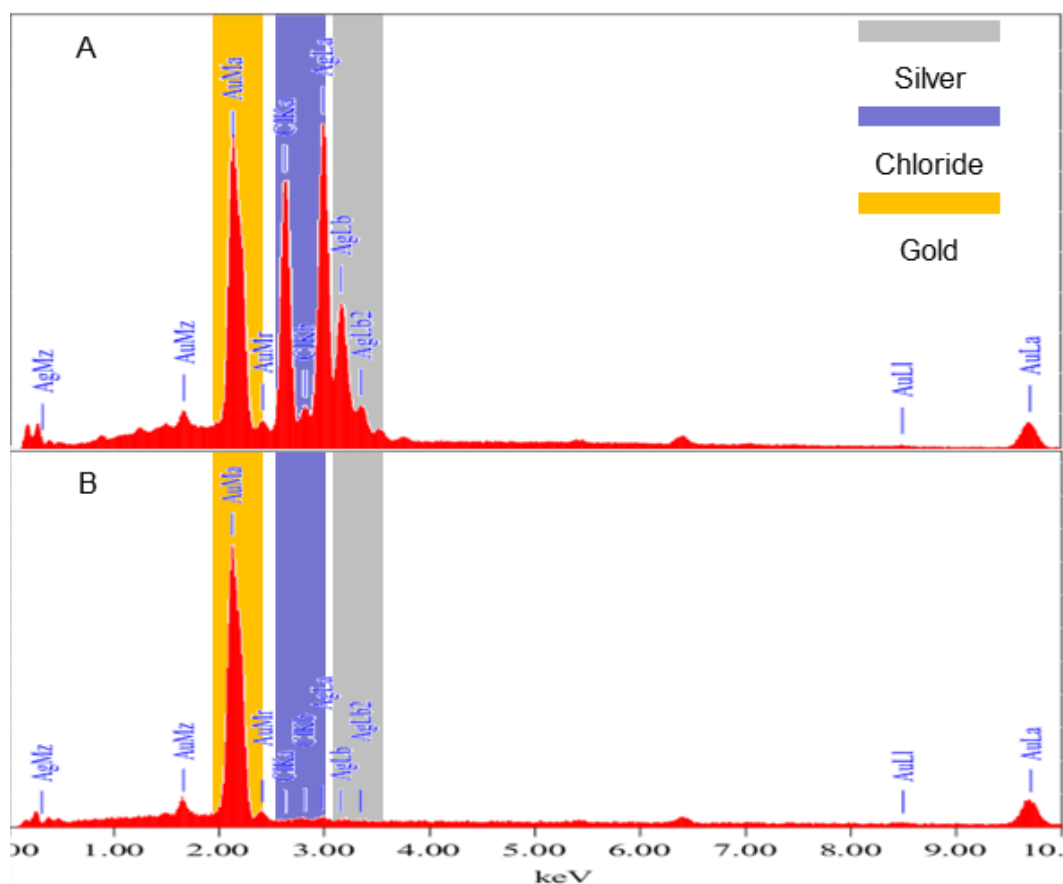


Figure 4.24 EDS spectra of Au/AgCl composites and CLGPs

4.3.5. Proposed circle galvanic replacement reaction mechanism.

Schematic diagram of circle galvanic replacement reaction showed in Figure 4.25. The film is automatically detached from the sacrificed silver plate as the film becomes thicker under ultrasonic radiation. The mechanism of circle galvanic replacement reaction could be explained auto ejection of the Au/AgCl composites: (A) original of a clean Ag metal before immersed to Au^{3+} solution, non-galvanic replacement reaction, (B) while clean Ag metal was dipped into Au^{3+} solution, Rapid epitaxial growth of Au film on the clean Ag surface, (C) precipitation and formation of AgCl precipitates was formed on Au film and, (D) Au/AgCl nanocomposites when prolong galvanic reaction, (E) AgCl underlay start development under Au/AgCl nanocomposites, (F) ultrasonic assisted detachment of the (galvanic generated) interpenetrated Au/AgCl nanocomposites film with AgCl underlay from the silver plate.

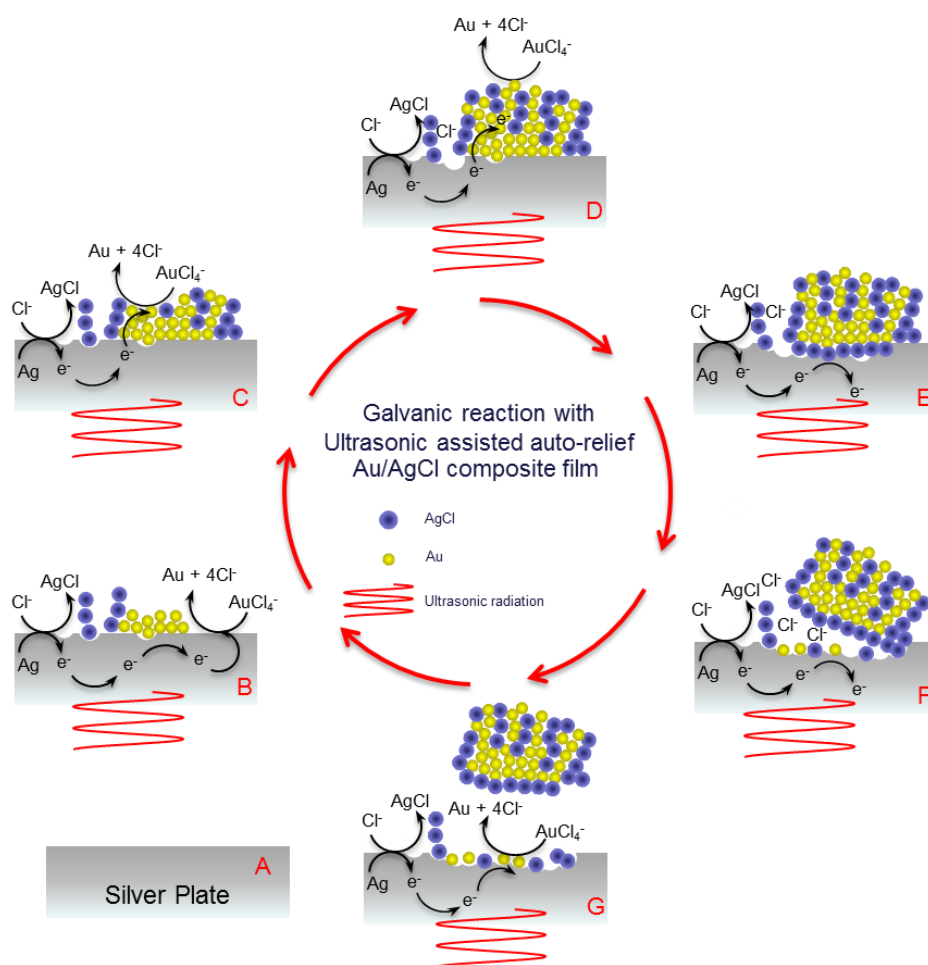


Figure 4.25 Schematic diagram of circle galvanic replacement reaction show the film is automatically detached from the sacrificed silver plate, *i.e.*, as the film becomes thicker. The mechanism of the nanoporous gold film development included: (A) supply/regeneration of a clean Ag surface (B) rapid epitaxial growth of Au film on the clean Ag surface (C) precipitation and formation of AgCl precipitates on Au film (D) formation of interpenetrated Au/AgCl nanocomposite (E) development of AgCl underlay (F) ultrasonic assisted detachment of the (galvanic generated) interpenetrated Au/AgCl nanocomposite film with AgCl underlay from the silver plate. The detachment occurs at the interface between Ag plate and the AgCl underlay. The ultrasonic assisted auto-detachment enables a self-initiated formation of clean Ag surface of the silver plate.

4.3.6. Surface enhanced Raman scattering (SERS) activity of CLGPs

The SERS studies were done by using a DXR Raman microscope. The SL crystals were transferred to a thin glass plate, washed with ethanol, and dried under ambient conditions. The SERS measurements were using crystal violet (CV) and rhodamine 6G (R6G) as the Raman probe molecule. The various concentrations of CV and R6G solutions were prepared in water at (10^{-3} - 10^{-6} M). The 1 μ L of standing CLGPs were dropped in glass slide and dried under vacuum condition. After that the 1 μ L required concentration of R6G and CV were dropped on standing CLGPs and dried under vacuum condition. Figure 4.8 and 4.9 show the SERS spectra of R6G and CV collected from the surface standing CLGPs using 532 nm excitation lasers with 1s acquisition time. All the peaks of R 6G and CV have been assigned in Table 1 and 2.

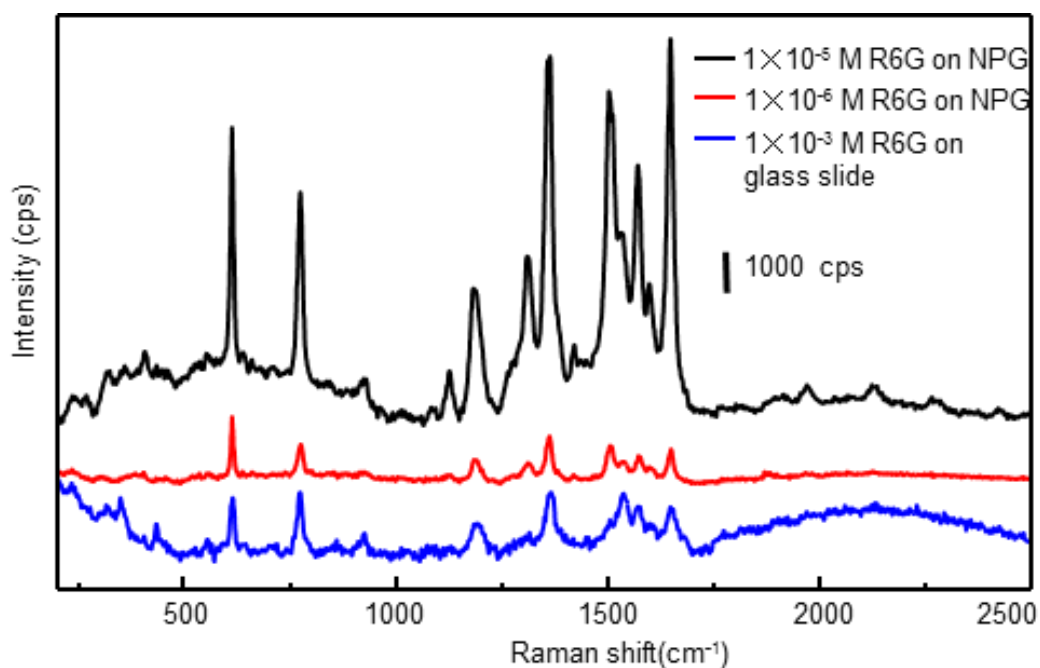


Figure 4.26 SERS of 1×10^{-5} and 1×10^{-6} M R6G on CLNPs compared with 1×10^{-3} M R6G on glass slide.

Table 4.1. Assignment of Raman bands of the SERS spectrum of R6G [72]

Raman band assignment	Raman shift (cm^{-1})
Xanthenes ring stretching, in plane C-H bending	1647
Xanthenes ring stretching, in plane N-H bending	1571
Xanthenes ring stretching, C-N stretching, C-H bending, N-H bending	1508
Xanthenes ring stretching, in plane C-H bending	1360
In plane xanthenes ring breathing	
N-H bending, CH_2 wagging	1309
In plane xanthenes ring deformation, C-H bending, N-H bending	1181
Out of plane C-H bending	770

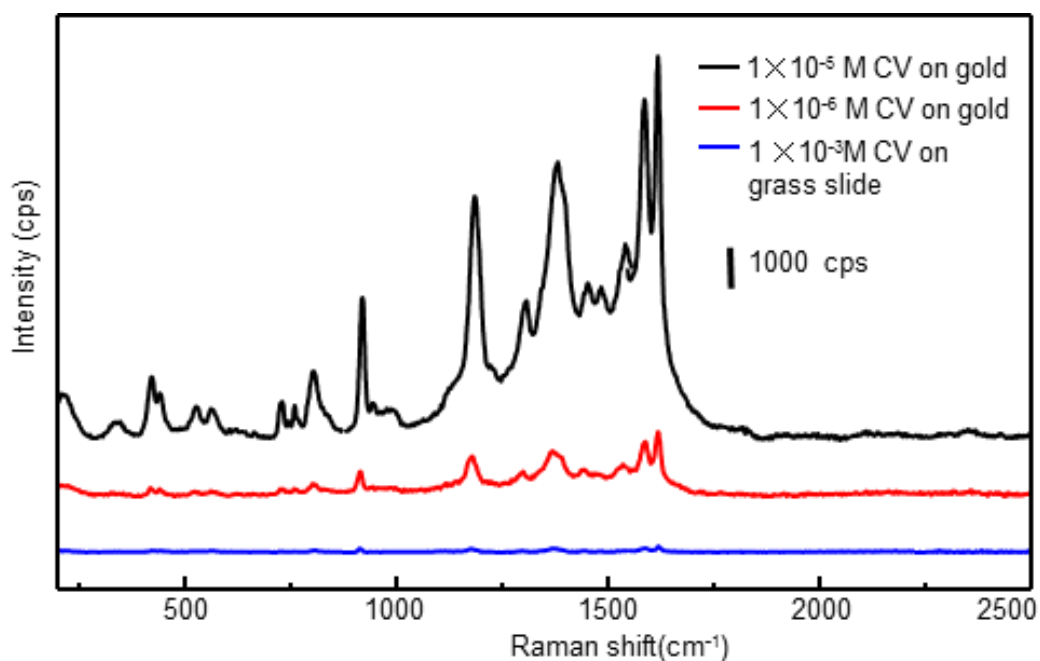
Figure 4.27 SERS of 1×10^{-5} and 1×10^{-6} M CV on CLNPs compared with 1×10^{-3} M R6G on glass slide

Table 4.2. Assignment of Raman bands of the SERS spectrum of CV [73]

Raman band assignment	Raman shift (cm ⁻¹)
ring C-C stretching	1627
ring C-C stretching	1592
ring C-C stretching	1542
+ ring deformation	1484
ring C-C stretching	1450
N-phenyl stretching	1379
ring C-C stretching	1305
ring C-H bend (II)	1186
ring C-H bend (II)	1131
ring skeletal vib. of radical orientation	992
ring skeletal vib. of radical orientation	922
ring C-H bend (⊥)	819
ring C-H bend (⊥)	768
ring C-H bend (⊥)	738
ring skeletal vib. of radical orientation	633
ring skeletal vib. of radical orientation	572
ring skeletal vib. of radical orientation	538
Ph-C+-Ph bend(⊥)	432
Ph-C+-Ph bend(II)	348
Breathing of central bonds	232
(II) and (⊥) means in-plane and out-of-plane, respectively	

CHAPTER V

CONCLUSIONS

Complex gold micro/nanostructures including coral-liked, needle-liked, Zen stone-liked gold nanostructures, and coral-liked gold micro/nanoporous film was synthesized by galvanic replacement reaction between a sacrificed silver metal and gold (III) ion (Au^{3+}) without stabilizer, capping agent. The complex structures could be controlled by tuning environmental conditions (*i.e.*, gold (III) ion condition, immersion time, chloride ion concentration, pH, and ultrasonic radiation). The coral-liked gold nanostructures with plate thinness size of 40-60 nm prefer grew on the gold film at 5,000 ppm of Au^{3+} solution, pH = 0, without excess Cl^- . But Needle-liked gold nanostructures with tips diameter of 20-50 nm grew with 2 M NaCl. In the case of Zen stone-liked gold microstructures size was controlled by pH of Au^{3+} solution. At pH 7, Zen stone-liked gold microstructures was developed on silver surface and absent the structures while increased pH of Au^{3+} solution to 14. The structural evolutions of coral-liked gold nanostructures were observed by scanning electron microscope (SEM) with energy dispersive X-ray spectroscopy (EDS). The epitaxial growth of gold film on the surface of silver was interfered by the precipitated AgCl that case to Au/AgCl composites. Excess Cl^- was added into Au^{3+} solution that reacted with AgCl transforming to soluble AgCl_2^- . The soluble species play an important role on the evolution needle-liked gold nanostructures. The micro channels of AgCl layer was observed on coral-liked and needle-liked gold nanostructures that assisted to mass, Au^{3+} , Cl^- , and Ag^+ , transform of the reaction. The ultrasonic also induced an auto-detachment of the galvanic generated film along the Au/AgCl interface. The complex gold nanostructures with nanoporous morphology were realized once the co-developed AgCl was removed. Coral-liked gold micro/nanoporous express high SERS detection up to 10^{-6} M rhodamine 6G (R6G) and crystal violet (CV).

All in all, the objectives of this research are fully fulfilled.

REFERENCES

- [1] Wittstock, A., Zielasek, V., Biener, J., Friend, C.M., and Bäumer, M. Nanoporous gold catalysts for selective gas-phase oxidative coupling of methanol at low temperature. Science 327 (2010): 319-322.
- [2] Tavakkoli, N., Nasrollahi, S., and Vatankhah, G. Electrocatalytic determination of ascorbic acid using a palladium coated nanoporous gold film electrode. Electroanalysis 24 (2012): 368-375.
- [3] Shulga, O.V., others. Preparation and characterization of porous gold and its application as a platform for immobilization of acetylcholine esterase. Chem. Mater. 19 (2007): 3902-3911.
- [4] Ahmadalinezhad, A., and Chen, A. High-performance electrochemical biosensor for the detection of total cholesterol. Biosens. Bioelectron. 26 (2011): 4508-4513.
- [5] Wang, J. Electrochemical glucose biosensors. Chem. Rev. 108 (2008): 814-25.
- [6] Sun, Y., and Xia, Y. Increased sensitivity of surface plasmon resonance of gold nanoshells compared to that of gold solid colloids in response to environmental changes. Anal. Chem. 74 (2002): 5297-5305.
- [7] Doering, W.E., and Nie, S. Single-molecule and single-nanoparticle sers: examining the roles of surface active sites and chemical enhancement. J. Phys. Chem. B 106 (2002): 311-317.
- [8] Nie, S., and Emory, S.R. Probing single molecules and single nanoparticles by surface-enhanced Raman scattering. Science 275 (1997): 1102-1106.
- [9] Kim, F., Sohn, K., Wu, J. ,and Huang, J. Chemical Synthesis of Gold Nanowires in Acidic Solutions. J. Am. Chem. Soc. 130 (2008): 14442-14443.
- [10] Soejima, T., and Kimizuka, N. One-pot room-temperature synthesis of single-crystalline gold nanocorolla in water. J. Am. Chem. Soc. 131 (2009): 14407-14412.
- [11] Guo, Z., others. Layered assemblies of single crystal gold nanoplates: direct room temperature synthesis and mechanistic study. J. Phys. Chem. C 112 (2008): 12638-12645.

- [12] Wang, D., Huang, J., Liu, Y., Han, X., and You, T. Facile synthesis and electrochemical properties of octahedral gold nanocrystals. J. Nanopart. Res. 13 (2011): 157-163.
- [13] Li, C., others. High-yield synthesis of single-crystalline gold nano-octahedra. Angew. Chem. Int. Ed. 46 (2007): 3264-3268.
- [14] Bechelany, M., others. Simple synthetic route for sers-active gold nanoparticles substrate with controlled shape and organization. Langmuir 26 (2010): 14364-14371.
- [15] Guerrero-Martínez, A., Barbosa, S., Pastoriza-Santos, I., and Liz-Marzán, L.M. Nanostars shine bright for you: colloidal synthesis, properties and applications of branched metallic nanoparticles. Curr. Opin. Colloid Interface Sci. 16 (2011): 118-127.
- [16] Fang, J., others. Gold mesostructures with tailored surface topography and their self-assembly arrays for surface-enhanced Raman spectroscopy. Nano Lett. 10 (2010): 5006-5013.
- [17] Qin, Y., others. Ionic liquid-assisted growth of single-crystalline dendritic gold nanostructures with a three-fold symmetry. Chem. Mater. 20 (2008): 3965-3972.
- [18] Mceachran, M., others. Ultrathin gold nanoframes through surfactant-free templating of faceted pentagonal silver nanoparticles. J. Am. Chem. Soc. 133 (2011): 8066-8069.
- [19] Moon, G.D., others. A new theranostic system based on gold nanocages and phase-change materials with unique features for photoacoustic imaging and controlled release. J. Am. Chem. Soc. 133 (2011): 4762-4765.
- [20] Sajanalal, P.R., Sreeprasad, T.S., Samal, A.K., and Pradeep, T., Anisotropic nanomaterials: structure, growth, assembly, and functions. Nano Reviews 2 (2011): 1-62.
- [21] Kelly, K.L., Coronado, E., Zhao, L.L., and Schatz, G.C. The optical properties of metal nanoparticles: the influence of size, shape, and dielectric environment. J. Phys. Chem. B 107 (2003): 668-677.

- [22] You, E.-A., Zhou, W., Suh, J.Y., Huntington, M.D., and Odom, T.W. Polarization-dependent multipolar plasmon resonances in anisotropic multiscale Au particles. ACS Nano 6 (2012): 1786-1794.
- [23] Rang, M., others. Optical near-field mapping of plasmonic nanoprisms. Nano Lett. 8 (2008): 3357-3363.
- [24] Wang, L., others. Photochemical synthesis and self-assembly of gold nanoparticles. Colloids Surf., A 312 (2008): 148-153.
- [25] Tessier, P.M., others. Assembly of gold nanostructured films templated by colloidal crystals and use in surface-enhanced Raman spectroscopy. J. Am. Chem. Soc. 122 (2000): 9554-9555.
- [26] Tseng, K.-H., Huang, J.-C., Liao, C.-Y., Tien, D.-C., and Tsung, T.-T. Preparation of gold ethanol colloid by the arc discharge method. J. Alloys Compd. 472 (2009): 446-450.
- [27] Lung, J.-K., others. Preparation of gold nanoparticles by arc discharge in water. J. Alloys Compd. 434-435 (2007): 655-658.
- [28] Journet, C., others. Large-scale production of single-walled carbon nanotubes by the electric-arc technique. Nature 388 (1997): 756-758.
- [29] Magnusson, M.H., Deppert, K., Malm, J.-O., Bovin, J.-O., and Samuelson, L. Size-selected gold nanoparticles by aerosol technology. Nanostruct. Mater. 12 (1999): 45-48.
- [30] Zeng, H., others. Nanomaterials via Laser Ablation/Irradiation in Liquid: a review. Adv. Funct. Mater. 22 (2012): 1333-1353.
- [31] Lee, P.C., and Meisel, D. Adsorption and surface-enhanced Raman of dyes on silver and gold sols. J. Phys. Chem. 86 (1982): 3391-3395.
- [32] Jana, N.R., Gearheart, L., and Murphy, C.J. Wet chemical synthesis of high aspect ratio cylindrical gold nanorods. J. Phys. Chem. B 105 (2001): 4065-4067.
- [33] Gao, J., Bender, C.M., and Murphy, C.J. Dependence of the gold nanorod aspect ratio on the nature of the directing surfactant in aqueous solution. Langmuir 19 (2003): 9065-9070.

- [34] Wei, Z., Mieszawska, A.J., and Zamborini, F.P. Synthesis and manipulation of high aspect ratio gold nanorods grown directly on surfaces. Langmuir 20 (2004): 4322-4326.
- [35] Wu, H.-L., Kuo, C.-H., and Huang, M.H. Seed-mediated synthesis of gold nanocrystals with systematic shape evolution from cubic to trisoctahedral and rhombic dodecahedral structures. Langmuir 26 (2010): 12307-12313.
- [36] Ye, X., others. Improved size-tunable synthesis of monodisperse gold nanorods through the use of aromatic additives. ACS Nano 6 (2012): 2804-2817.
- [37] Desantis, C.J., Sue, A.C., Bower, M.M., and Skrabalak, S.E. Seed-mediated co-reduction: a versatile route to architecturally controlled bimetallic nanostructures. ACS Nano 6 (2012): 2617-2628.
- [38] Sun, Y., Yin, Y., Mayers, B.T., Herricks, T., and Xia, Y. Uniform silver nanowires synthesis by reducing AgNO_3 with ethylene glycol in the presence of seeds and poly(vinyl pyrrolidone). Chem. Mater. 14 (2002): 4736-4745.
- [39] Sun, Y., and Xia, Y. Shape-controlled synthesis of gold and silver nanoparticles. Science 298 (2002): 2176-2179.
- [40] Silvert, P.Y., and Tekaiia-Elhsissen, K. Synthesis of monodisperse submicronic gold particles by the polyol process. Solid State Ionics 82 (1995): 53-60.
- [41] Lu, X., Rycenga, M., Skrabalak, S.E., Wiley, B., and Xia, Y. Chemical synthesis of novel plasmonic nanoparticles. Annu. Rev. Phys. Chem. 60 (2009): 167-192.
- [42] Dong, S.-A., and Zhou, S.-P. Photochemical synthesis of colloidal gold nanoparticles. Mater. Sci. Eng., B 140 (2007): 153-159.
- [43] Esumi, K., Matsuhisa, K., and Torigoe, K. Preparation of rodlike gold particles by UV irradiation using cationic micelles as a template. Langmuir 11 (1995): 3285-3287.
- [44] Huang, W.-C., and Chen, Y.-C. Photochemical synthesis of polygonal gold nanoparticles. J. Nanopart. Res. 10 (2008): 697-702.

- [45] Gutierrez, M., Henglein, A., and Dohrmann, J.K. Hydrogen atom reactions in the sonolysis of aqueous solutions. J. Phys. Chem. 91 (1987): 6687-6690.
- [46] Okitsu, K., others. Formation of noble metal particles by ultrasonic irradiation. Ultrason. Sonochem. 3 (1996): S249-S251.
- [47] Makino, K., Mossoba, M.M., and Riesz, P. Chemical effects of ultrasound on aqueous solutions. Evidence for hydroxyl and hydrogen free radicals (.cntdot.OH and .cntdot.H) by spin trapping. J. Am. Chem. Soc. 104 (1982): 3537-3539.
- [48] Sakai, T., Enomoto, H., Torigoe, K., Sakai, H., and Abe, M. Surfactant- and reducer-free synthesis of gold nanoparticles in aqueous solutions. Colloids Surf., A 347 (2009): 18-26.
- [49] Radziuk, D., others. Ultrasound-assisted fusion of preformed gold nanoparticles. J. Phys. Chem. C 114 (2010): 1835-1843.
- [50] Suslick, K.S., Hammerton, D.A., and Cline, R.E. Sonochemical hot spot. J. Am. Chem. Soc. 108 (1986): 5641-5642.
- [51] Muthukumaran, S., others. The optimisation of ultrasonic cleaning procedures for dairy fouled ultrafiltration membranes. Ultrason. Sonochem. 12 (2005): 29-35.
- [52] Chatterjee, D. Use of ultrasonics in shear layer cavitation control. Ultrasonics 41 (2003): 465-475.
- [53] Sun, Y., and Xia, Y. Mechanistic study on the replacement reaction between silver nanostructures and chloroauric acid in aqueous medium. J. Am. Chem. Soc. 126 (2004): 3892-3901.
- [54] Kwon, S., Dong, H., and Lee, S.-Y. Study of the reaction rate of gold nanotube synthesis from sacrificial silver nanorods through the galvanic replacement method. Journal of Nanomaterials 2010 (2010): 1-7.
- [55] Au, L., others. Synthesis and optical properties of cubic gold nanoframes. Nano Res. 1 (2008): 441-449.
- [56] Sayed, S.Y., others. Heteroepitaxial growth of gold nanostructures on silicon by galvanic displacement. ACS Nano 3 (2009): 2809-2817.

- [57] Wang, Y., others. Nanostructured gold films for sers by block copolymer-templated galvanic displacement reactions. Nano Lett. 9 (2009): 2384-2389.
- [58] Sayed, S.Y., and Buriak, J.M. Epitaxial growth of nanostructured gold films on germanium via galvanic displacement. ACS Appl. Mater. Interfaces 2 (2010): 3515-3524.
- [59] Gutés, A., Carraro, C., and Maboudian, R. Ultrasooth gold thin films by self-limiting galvanic displacement on silicon. ACS Appl. Mater. Interfaces 3 (2011): 1581-1584.
- [60] Zhang, X., Qiao, Y., Xu, L., and Buriak, J.M. constructing metal-based structures on nanopatterned etched silicon. ACS Nano 5 (2011): 5015-5024.
- [61] Liang, X., Wang, Z.-J., and Liu, C.-J. Size-controlled synthesis of colloidal gold nanoparticles at room temperature under the influence of glow discharge. Nanoscale Res. Lett. 5 (2009): 124 - 129.
- [62] Kim, Y.-G., Oh, S.-K., and Crooks, R.M. preparation and characterization of 1–2 nm dendrimer-encapsulated gold nanoparticles having very narrow size distributions. Chem. Mater. 16 (2003): 167-172.
- [63] Brevnov, D.A., Olson, T.S., López, G.P., and Atanassov, P. Electroless deposition of silver by galvanic displacement on aluminum alloyed with copper. J. Phys. Chem. B 108 (2004): 17531-17536.
- [64] Wang, D., Li, T., Liu, Y., Huang, J., and You, T. Large-scale and template-free growth of free-standing single-crystalline dendritic ag/pd alloy nanostructure arrays. Cryst. Growth Des. 9 (2009): 4351-4355.
- [65] Zelyanskii, A.V., Zhukova, L.V., and Kitaev, G.A. Solubility of AgCl and AgBr in HCl and HBr. Inorg. Mater. 37 (2001): 523-526.
- [66] Lampre, I., Pernot, P., and Mostafavi, M. Spectral properties and redox potentials of silver atoms complexed by chloride ions in aqueous solution. J. Phys. Chem. B 104 (2000): 6233-6239.
- [67] Fritz, J.J. Thermodynamic properties of chloro-complexes of silver chloride in aqueous solution. J. Solution Chem. 14 (1985): 865-879.

- [68] Stognij, A., Novitskii, N., Tushina, S., and Kalinnikov, S. Preparation of ultrathin gold films by oxygen-ion sputtering and their optical properties. Tech. Phys. 48 (2003): 745-748.
- [69] Ng, F.L., Wei, J., Lai, F.K., and Goh, K.L. Metallic thin film depth measurements by X-ray microanalysis. Appl. Surf. Sci. 252 (2006): 3972-3976.
- [70] Gong, X., Yang, Y., and Huang, S. A Novel Side-Selective Galvanic Reaction and Synthesis of Hollow Nanoparticles with an Alloy Core. J. Phys. Chem. C 114 (2010): 18073-18080.
- [71] Sun, Y. Conversion of Ag nanowires to AgCl nanowires decorated with Au nanoparticles and their photocatalytic activity. J. Phys. Chem. C 114 (2010): 2127-2133.
- [72] Yang, Y.-C., others. Electrochemical growth of gold nanostructures for surface-enhanced Raman scattering. J. Phys. Chem. C 115 (2011): 1932-1939.
- [73] Shibu, E.S., Kimura, K., and Pradeep, T. Gold nanoparticle superlattices: novel surface enhanced Raman scattering active substrates. Chem. Mater. 21 (2009): 3773-3781.

VITAE**Name:** Mr. Prasert Sornprasit**Date of Birth:** March 16, 1985 **Birth place:** Songkhla, Thailand**Address:** 11 Moo 5 Kare Sub District, Chana District, Songkhla 90130
Thailand, E-mail address: Sert_krab@hotmail.com**Education:**

2008 Bachelor of Science in Chemistry
 Prince of Songkla University, Thailand

2012 Master of Science in Chemistry
 Chulalongkorn University, Thailand

Conferences:

26-28 October 2010	36th Congress on Science and Technology of Thailand
5-7 January 2011	28th Annual Conference of the Microscopy Society of Thailand
30 January- 1 February 2012	29th Annual Conference of the Microscopy Society of Thailand